Article

Current Biology

Mechanosensory bristles mediate avoidance behavior by triggering sustained local motor activity in *Drosophila melanogaster*

Graphical abstract

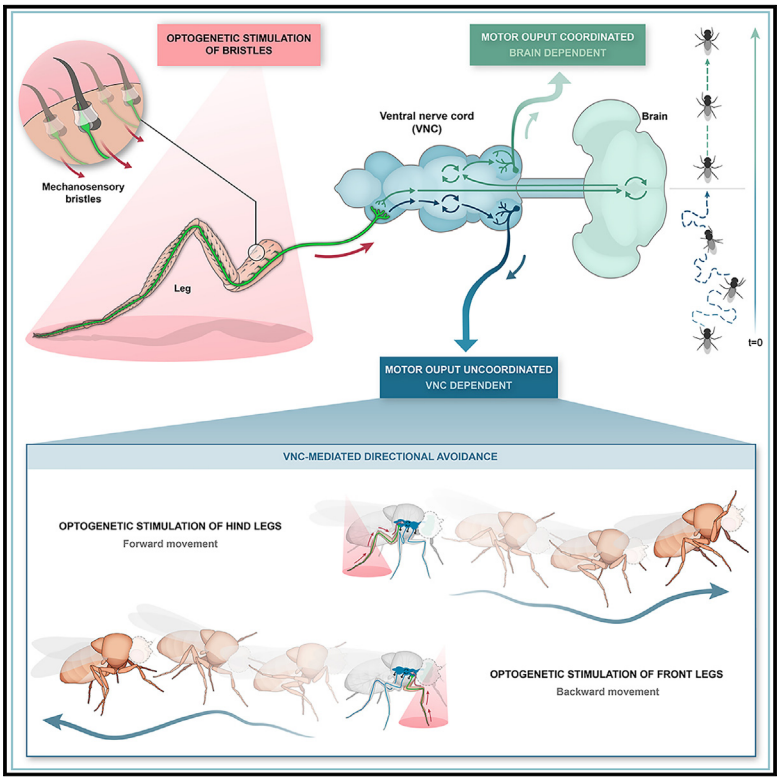

Highlights

- Leg mechanosensory bristle activation elicits a brain-independent motor response
- Bristle-evoked movement encompasses an initial fast uncoordinated phase
- Bristle stimulation leads to a directional avoidance response
- Directional avoidance can be mediated by the VNC without central brain involvement

Authors

Alexandra M. Medeiros, Anna F. Hobbiss, Gonçalo Borges, Marta Moita, César S. Mendes

Correspondence

cesar.mendes@nms.unl.pt

In brief

In this study, Medeiros et al. show that activation of leg mechanosensory bristles directly triggers motor circuits within the fly's ventral nerve cord, causing sustained and directional motor activity independently of higher-order circuits. This fast but uncoordinated response can form the basis for a sensory-evoked avoidance behavior.

Medeiros et al., 2024, Current Biology *34*, 1–19
July 8, 2024
https://doi.org/10.1016/j.cub.2024.05.021

CellPress

Current Biology

CellPress

Article

Mechanosensory bristles mediate avoidance behavior by triggering sustained local motor activity in *Drosophila melanogaster*

Alexandra M. Medeiros,[1] Anna F. Hobbiss,[1,2] Gonçalo Borges,[1] Marta Moita,[2] and César S. Mendes[1,3,*]
[1]iNOVA4Health, NOVA Medical School|Faculdade de Ciências Médicas, NMS|FCM, Universidade Nova de Lisboa, 1169-056 Lisbon, Portugal
[2]Champalimaud Research, Champalimaud Center for the Unknown, 1400-038 Lisbon, Portugal
[3]Lead contact
*Correspondence: cesar.mendes@nms.unl.pt
https://doi.org/10.1016/j.cub.2024.05.021

SUMMARY

During locomotion, most vertebrates—and invertebrates such as *Drosophila melanogaster*—are able to quickly adapt to terrain irregularities or avoid physical threats by integrating sensory information along with motor commands. Key to this adaptability are leg mechanosensory structures, which assist in motor coordination by transmitting external cues and proprioceptive information to motor centers in the central nervous system. Nevertheless, how different mechanosensory structures engage these locomotor centers remains poorly understood. Here, we tested the role of mechanosensory structures in movement initiation by optogenetically stimulating specific classes of leg sensory structures. We found that stimulation of leg mechanosensory bristles (MsBs) and the femoral chordotonal organ (ChO) is sufficient to initiate forward movement in immobile animals. While the stimulation of the ChO required brain centers to induce forward movement, unexpectedly, brief stimulation of leg MsBs triggered a fast response and sustained motor activity dependent only on the ventral nerve cord (VNC). Moreover, this leg-MsB-mediated movement lacked inter- and intra-leg coordination but preserved antagonistic muscle activity within joints. Finally, we show that leg-MsB activation mediates strong avoidance behavior away from the stimulus source, which is preserved even in the absence of a central brain. Overall, our data show that mechanosensory stimulation can elicit a fast motor response, independently of central brain commands, to evade potentially harmful stimuli. In addition, it sheds light on how specific sensory circuits modulate motor control, including initiation of movement, allowing a better understanding of how different levels of coordination are controlled by the VNC and central brain locomotor circuits.

INTRODUCTION

Moving organisms possess highly efficient motor circuits that integrate multisensorial information and execute the appropriate motor response.[1,2] This is particularly necessary when facing irregular terrain and avoiding obstacles and collisions.[3–5] In insects, including *Drosophila*, descending interneurons (DNs) bridge the central brain and gnathal ganglia (GNG) with executive circuits in the ventral nerve cord (VNC), the insect equivalent of the mammalian spinal cord, controlling a plethora of motor behaviors, including locomotion.[6–9] These circuits can quickly adapt to external environmental conditions, optimizing speed, stability, and energy consumption.[1,2] Mechanosensory feedback mechanisms, including proprioception (internal sense of position and movement) and exteroception (perception of external stimuli), are key to this flexibility. These sensory functions are enabled by specialized neurons that relay physical features, such as muscle extension, tissue compression, or gravitational orientation to motor centers. Their absence renders animals highly "uncoordinated," largely determined by the number and class of inactivated cells.[10,11] Sensory structures vary in shape and properties depending on the type of mechanical feature being transduced.[12] For example, in insects, the chordotonal organ (ChO) relays mechanical features of joints, in a manner analogous to mammalian muscle spindles.[13] Among exteroceptors, mechanosensory bristles (MsBs) are involved in detecting external cues, such as dust particles, parasites, and wind intensity, triggering varied motor outcomes, such as grooming, defensive kicking, or locomotion arrest.[14–16] Moreover, direct mechanical or optogenetic stimulation of MsBs induces a reflexive postural adjustment or avoidance away from the stimulation site.[17–19]

Each MsB is connected to the dendrites of a mechanosensory neuron, whose axon projects to the ventral-most layer of the leg neuropil within the VNC, where sensory information is processed.[13,14,20] The local circuits responsible for processing mechanosensory receptive fields comprise a complex network of excitatory and inhibitory synapses, which are capable of targeting motor neurons.[21,22] Evidence shows that sensory structures can directly affect ongoing muscle contraction locally to correct

Please cite this article in press as: Medeiros et al., Mechanosensory bristles mediate avoidance behavior by triggering sustained local motor activity in *Drosophila melanogaster*, Current Biology (2024), https://doi.org/10.1016/j.cub.2024.05.021

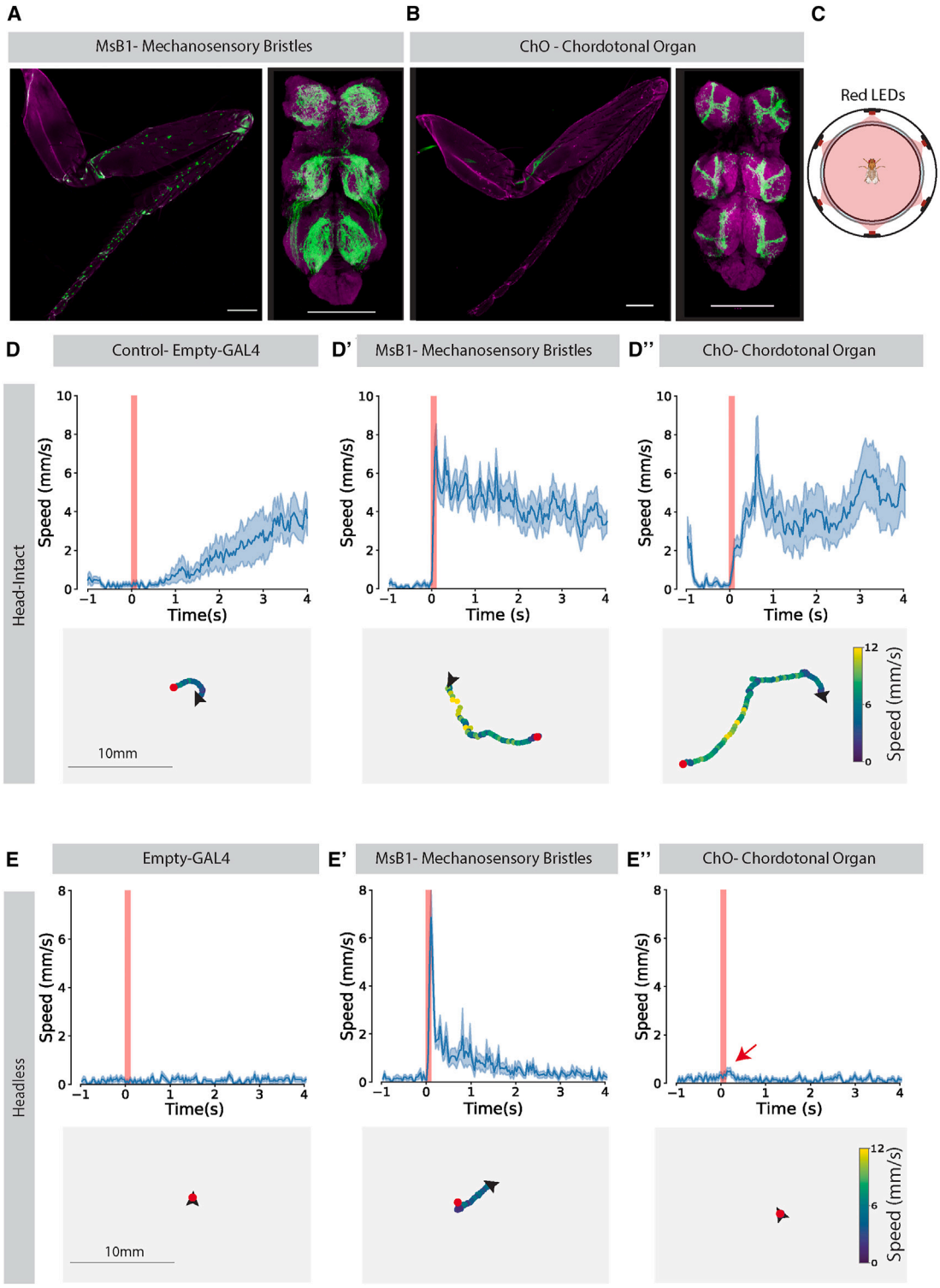

Figure 1. Optogenetic stimulation of leg mechanosensory bristles triggers movement in stationary flies

(A) Leg and VNC expression patterns of MsB1 line. mVenus expression under combinatorial control of R65D12 and dac^{RE}-flp. Genotype: R65D12-GAL4, dac^{RE}-flp, UAS-FRT-stop-FRT-Chrimson-mVenus. Cell bodies are located in the legs (left) and send axonal projections to the VNC (right). We ruled out labeling of chemosensory structures based on anatomy.[14,28,29] Scale bars, 100 μm.

(B) Leg and VNC expression pattern of ChO line. mVenus expression under combinatorial control of R79E02 and ato-flp. Genotype: R79E02-GAL4, ato-flp, UAS-FRT-stop-FRT-Chrimson-mVenus. Cell bodies are located in the legs (left) and send axonal projections to the VNC (right). Scale bars, 100 μm.

(C) Schematic of the behavioral arena. Arena is surrounded by six deep red LEDs. See STAR Methods for details.

(legend continued on next page)

Please cite this article in press as: Medeiros et al., Mechanosensory bristles mediate avoidance behavior by triggering sustained local motor activity in *Drosophila melanogaster*, Current Biology (2024), https://doi.org/10.1016/j.cub.2024.05.021

movement and posture. For instance, in the stick insect, sensory feedback from the ChO and campaniform sensilla assist in-phase transitions from stance to swing phase, termed "active reaction," which influences the activation threshold by flexor and extensor motor pools, providing a positive reinforcement of movement.[23,24] In the locust, leg tactile stimulation can elicit fictive motor activity resembling "walking" patterns.[25] Further studies suggest the existence of a local neuronal architecture within the VNC linking sensory structures to central pattern generators (CPGs) and leg motor neurons to produce intersegmental coordination.[26] These findings suggest the potential for leg mechanosensation to initiate sustained walking activity. Whether fly circuits substantiate this possibility, and whether mechanosensory class and location serve as determinants to drive walking activity, remains uncertain. To investigate this question, we took advantage of the rich genetic toolkit and quantitative kinematic tools available for *Drosophila*.

Here, we show that stimulation of MsBs or ChO is sufficient to initiate forward movement. Brief stimulation of the leg MsBs (but not the head or wing MsBs) elicited immediate and sustained motor activity independent of descending commands, which lacked inter- and intra-leg coordination. Finally, targeted stimulation of front and hindleg MsBs induced a strong and directional avoidance behavior, even in the absence of the central brain.

This study sheds light on the ability of specific sensory inputs to engage motor circuits within the VNC that provide directional movement, while highlighting the necessity of the central brain for inter- and intra-leg coordination during walking. These processes are particularly relevant in the context of avoidance behavior.

RESULTS

Activation of leg MsBs evokes brain-independent movement

To understand the role of leg sensory afferents in movement control and walking initiation, we identified fly lines from the Janelia Flylight collection targeting different types of mechanosensory neurons in the leg.[27] To restrict GAL4 expression to the legs, we used a combinatorial approach with flipase under the control of the dac^{RE} enhancer fragment.[11] We selected two lines, one labeling MsBs (hereafter termed MsB1) and one labeling the femoral ChO (termed ChO) (Figures 1A, 1B, and S1).

We tested the expression patterns of the selected lines and observed, as described previously, that MsB1 neurons project to the ventral-most layer of the leg neuropil, the ventral association center (VAC) (Figure S1A).[30] Projections from the ChO line targeted the medial ventral association layer (mVAC) and the intermediate neuropil (IntNP) (Figures 1B and S1B).[30] In the brain, we identified ChO axon terminals in the wedge (WED) region and the antennal mechanosensory and motor center (AMMC) (Figure S1B). The MsB1 line showed some labeling in the antennal lobes and GNG. We also found cell labeling in the maxillary palps, in the proboscis, and in the 3rd antennal segment (Figure S1A; data not shown), possibly explaining MsB1 labeling of brain structures.[14,31–33]

Next, we measured the behavioral responses of immobile flies to optogenetic stimulation of the selected lines. We drove expression of the light-gated CsChrimson channel and analyzed fly behavior after a single 100-ms stimulation in an open-field arena (Figure 1C; STAR Methods).[34] While control empty-GAL4 flies remained immobile immediately after stimulation, stimulation of MsB1 or ChO led to forward walking (Figures 1D and S1F; Video S1). Motor responses differed between these two lines, with MsB1 stimulation inducing a very short latency response, reaching a maximum speed of 7.38 ± 1.17 mm/s 60 ms after stimulus onset, while ChO stimulation led to a more progressive response, reaching maximum speed of 6.98 ± 1.99 mm/s after 600 ms (Figures 1D′ and D″, upper panels). We noticed that MsB1 stimulation triggered a startle response (a fast, short-latency motor response to a sudden unexpected stimulus)[35] characterized by an apparent uncoordinated locomotor pattern followed by sustained "coordinated" walking. In contrast, ChO stimulation led to an apparent coordinated walking pattern (Figures 1D′ and 1D″; Video S1), suggesting that ChO and MsBs promote movement using different neuronal circuits.

We then asked whether movement initiation was dependent on descending information by decapitating the animals before optogenetic stimulation (Figure 1E), which removes all descending inputs from the brain and GNG and all sensory feedback from the head capsule. Decapitated *Drosophila* can maintain an upright posture and display innate behaviors such as grooming.[17,36] While control animals (empty-GAL4) did not exhibit any optogenetic response (Figures 1E and S1F; data not shown), MsB1 stimulation triggered an immediate response phenocopying the uncoordinated startle seen in the head-intact animals, moving mainly forward (Figures 1E′ and S1F–S1H; Video S1) and reaching a peak speed of 6.85 ± 1.27 mm/s, 60 ms after stimulus onset, with motor activity sustained for approximately 2.9 s. In contrast, optogenetic stimulation of ChO in beheaded flies did not induce movement (Figures 1E″ and S1F), suggesting these sensory neurons require brain circuits for walking initiation. Flies exhibited a leg twitch reflex, which slightly shifted the body's centroid, likely resulting from direct synaptic connections between the ChO and leg motor neurons,[37] causing a small increase in the perceived instantaneous speed (red arrow in Figure 1E″; Video S1). We also tested nanchung-GAL4, a commonly used ChO driver,[38] which phenocopied the results observed with our ChO driver (Figure S1I).

These results indicate that stimulating mechanosensory structures in the leg is sufficient to initiate walking, which for MsB1 only depends on local circuits within the VNC. However, sustained walking after MsB stimulation requires descending activity from the brain.

(D and E) Instantaneous speed and trajectories over time after optogenetic stimulation. Upper panels show instantaneous speed over time, with red bar representing 100 ms red light stimulus. Dark blue line and light blue shadows indicate the average and SEM for all replicates, respectively. Lower panels show representative trajectories for 4 s after optogenetic stimulation. Trajectory plots are color coded according to the speed of the fly, with black arrows and red dots indicating the initial and final positions, respectively. (D) Head-intact and (E) headless animals. Red arrow indicates a brief speed increase due to leg twitch. N = 19∼20 animals for all conditions.
See also Figure S1 and Video S1.

Please cite this article in press as: Medeiros et al., Mechanosensory bristles mediate avoidance behavior by triggering sustained local motor activity in *Drosophila melanogaster*, Current Biology (2024), https://doi.org/10.1016/j.cub.2024.05.021

Movement triggered by MsB is leg specific

We next asked whether the motor response can also be triggered by MsBs in other body structures. Full-body stimulation of MsBs, achieved through dust particles or genetic means, induces grooming behavior.[16,39] In our study, restricting activation to leg MsBs resulted in mainly uncoordinated locomotion. Considering previous findings on compartmentalized sensory connections leading to different behavioral responses,[17,18] we asked whether the motor response depended on the location of the stimulus. For this, we used the same GAL4 driver combined with a head capsule or wing-specific flipase line using the eyeless (ey) and vestigial (vg) fragments, respectively (Figure 2A; STAR Methods). We confirmed the presence of positive cells in the respective cuticle and axonal projections (Figures S1C–S1E). We then cataloged the repertoire of motor behaviors in response to optogenetic stimulation using automatic and manual classifiers (STAR Methods).

In head-intact animals, leg MsB activation triggered an apparent uncoordinated locomotion, immediately followed by coordinated walking and grooming in most animals (12 out of 20) (Figure 2B). Conversely, head stimulation induced initiation of coordinated walking (Figures 2C–2E), possibly through antennal olfactory sensory neurons, which can drive forward walking.[40] Stimulation of wing MsBs led only a small fraction of the animals to groom (2 out of 20) compared with leg or head stimulation (11 and 10 out of 20, respectively) (Figures 2B–2E). These data show that the uncoordinated activation of leg motor centers is specific to leg afferents.

We then asked whether these behaviors require higher-order brain commands. As before, we found that leg MsB stimulation in headless animals led to uncoordinated body displacement (Figures 2F and 2H). Conversely, stimulation of wing MsB afferents in headless flies resulted instead in grooming, a behavior absent in head-intact conditions (Figure 2C). Video analysis of headless flies showed that the observed leg movement bouts sometimes resembled a defensive kick, described previously, to remove fictitious parasites[15] (Video S2). We also tested the possibility that a discrete subpopulation of leg cells could be sufficient to activate cyclic movement. Using six additional GAL4 lines expressed in a subset of bristles (ranging between 4 and 57), we characterized their response to optogenetic stimulation and found that even small groups of MsBs can drive uncoordinated behavior (Table S1; Figures S2C–S2E). We also found a notable correlation ($r = 0.44$) between duration of uncoordinated phase and the quantity of labeled cells in the femur, while other structures showed a low correlation with the uncoordinated phase ($r < 0.28$), suggesting that femur MsBs have a significant influence on the VNC-dependent leg movement.

Overall, our data show that the motor response triggered by sensory stimulation depends not only on the class of sensory receptor (MsBs) but also on the source of the stimulus and the number of cells recruited.

MsB stimulation evokes movement encompassing an uncoordinated phase

Next, we investigated the kinematic features of the MsB-induced response using the FlyWalker system, which quantifies kinematic parameters with high spatiotemporal resolution.[11,41,42]

Control animals display a typical tripod gait pattern (Figure 3A) and consistent stance traces (tarsal ground contacts relative to body axis) (Figure 3C), indicating high levels of leg coordination.[11,21,43–45] Leg MsB stimulation-induced forward movement displayed two visually distinct phases: an early uncoordinated phase followed by a late coordinated phase (Figures 3B and 3D and 3B′ and 3E, respectively; Video S3).

The uncoordinated phase displayed a fast and an apparent random step pattern without any clear coupling between the six legs (Figures 3B and 3D). Following the uncoordinated phase, the coordinated phase showed normal walking patterns. To better characterize the different phases of MsB-evoked movement, we analyzed the step configurations, a proxy for inter-leg coordination, and found a large proportion of frames that do not match any of the normal gaits or configurations described for control flies.[11,43,44,46] (Figures 3A and 3B, lower panels). We describe these configurations as "non-compliant" because they do not comply with the rules of coordinated movement.[47,48] These include, for example, two contralateral or two consecutive ipsilateral legs lifted simultaneously. Due to this unstable leg support caused by insufficient fly pad (or pulvilli) contacts, we noticed occasional ventral (and more proximal tarsal) contacts, which are absent in normal walking animals (Figures S3A–S3C; data not shown). We calculated that non-compliant configurations were notably prevalent during the uncoordinated phase (29.6% ± 4.4%), contrasting with their near absence in control animals (Figures 3F and S3D). We then analyzed features of the stance-like phases during the uncoordinated phase, defined as moments when the tarsi contact the ground, and swing-like phases when the leg is in the air. We found that the stance-like traces display highly variable and inconsistent leg contacts (Figures 3C–3E and 3G). Nevertheless, during the uncoordinated phase, leg retraction (i.e., backward movement relative to the body) is still largely present during the stance-like phase (Figures 3D and 3H). This pattern matches the standard leg movement that results in the forward displacement of the body. Furthermore, we evaluated the whole kinematic profile and found that most kinematic parameters were altered (Figure S3D).

During the transition from an uncoordinated to a distinct coordinated phase, most flies display a period during which all legs contact the ground, while the body is still in motion (19 out of 21, 90.4%) (Figure 3B; ∼1.4 s). From a total of 21 flies tested, 10 (48%) shifted to coordinated walking without stopping (e.g., Figures 3B and 3B′), 4 (19%) showed a small pause of 200 to 400 ms, and 6 (29%) flies initiated grooming for a significant period of time before resuming walking. Animals receiving sequential stimuli showed a similar trend (data not shown), suggesting that distinct signals are able to counteract the sensory-evoked uncoordinated phase. Once animals return to a coordinated phase, both gait patterns and stance traces become similar to control animals (Figures 3B′, 3E–3H, and S3D).

In summary, stimulation of leg MsBs results in a fast cyclic movement, during which flies display an uncoordinated phase, lacking inter-leg coordination, followed by a coordinated phase presenting the stereotypical properties of walking animals.

Please cite this article in press as: Medeiros et al., Mechanosensory bristles mediate avoidance behavior by triggering sustained local motor activity in *Drosophila melanogaster*, Current Biology (2024), https://doi.org/10.1016/j.cub.2024.05.021

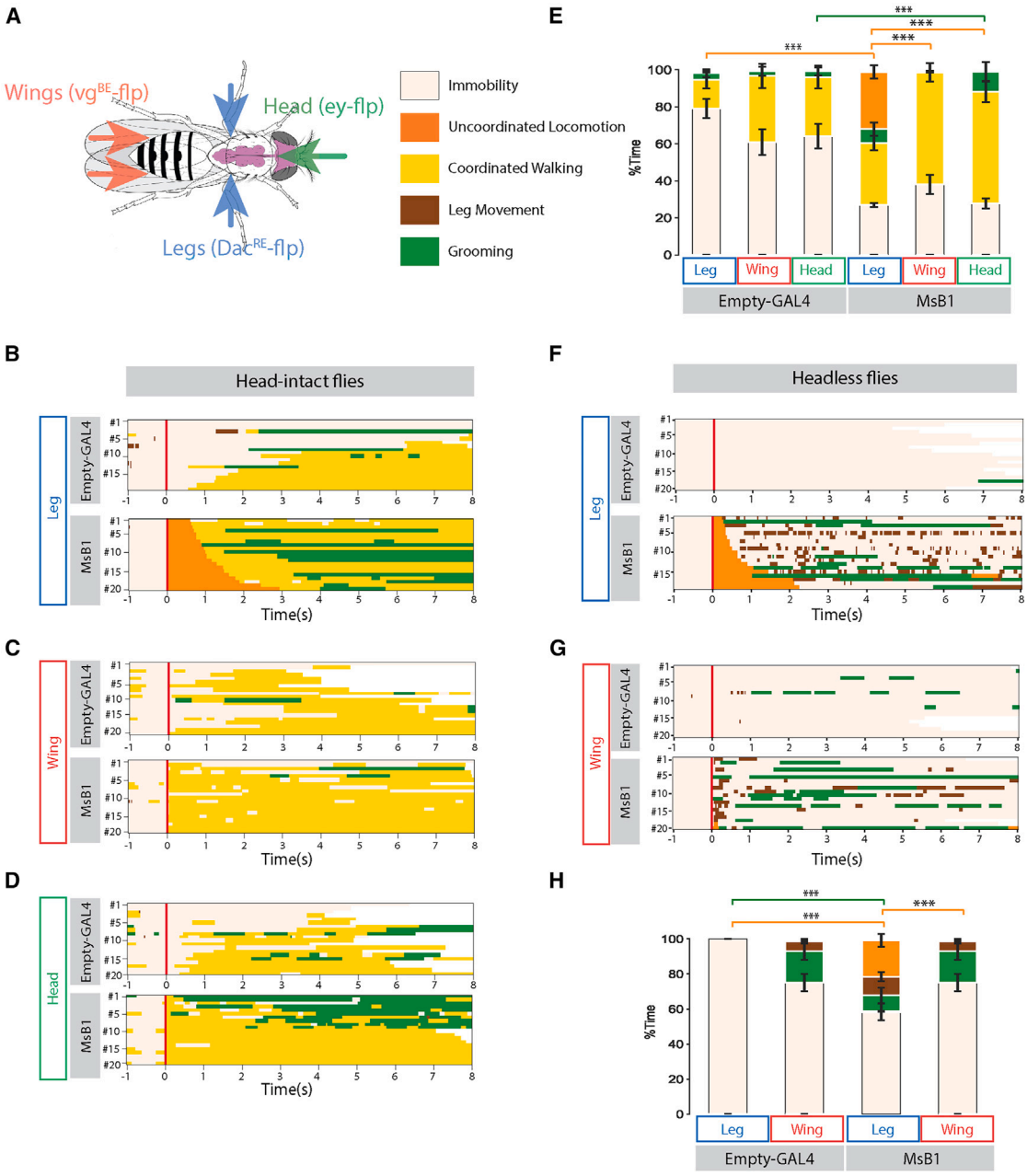

Figure 2. Cyclic movement is specific to leg mechanosensory bristle stimulation

(A) Schematic showing the combinatorial genetic tools used to restrict the expression of the MsB GAL4 driver R65D12 to the legs (dac^{RE}-flp), wings (Vg^{BE}-flp), and head (ey-flp) regions. Each combination was crossed with UAS>>CsChrimson.

(B–D, F, and G) Raster plots illustrating the flies' movement within 1 s before and after the stimulation of leg MsB. The x axis denotes time in seconds, with 0 indicating the precise moment of stimulation by red light pulse (red bar). Each line corresponds to one individual. Movement categories: immobility (beige), uncoordinated locomotion (orange), coordinated walking (yellow), leg movement (brown), and grooming (green). Upper panel shows empty-GAL4 behavior, while lower panel shows MsB1 GAL4 (R65D12) behavior.

(B–D) Head-intact animals. (B) Leg domain (with dac^{RE}-flp). (C) Wing domain (with Vg^{BE}-flp). (D) Head domain (with ey-flp).

(F and G) Headless animals. (F) Leg domain. (G) Wing domain.

(E and H) Stacked bar plots depicting the percentage of time allocated to behaviors described earlier within a 3-s window post stimulation for head-intact (E) and headless flies (H). Statistical analysis with Kruskal-Wallis ANOVA followed by Dunn's post hoc analysis: $^{*}p < 0.05$ $^{**}p < 0.01$, $^{***}p < 0.001$. $n = 20$ for all conditions. See also Figure S2, Video S2, and Table S1.

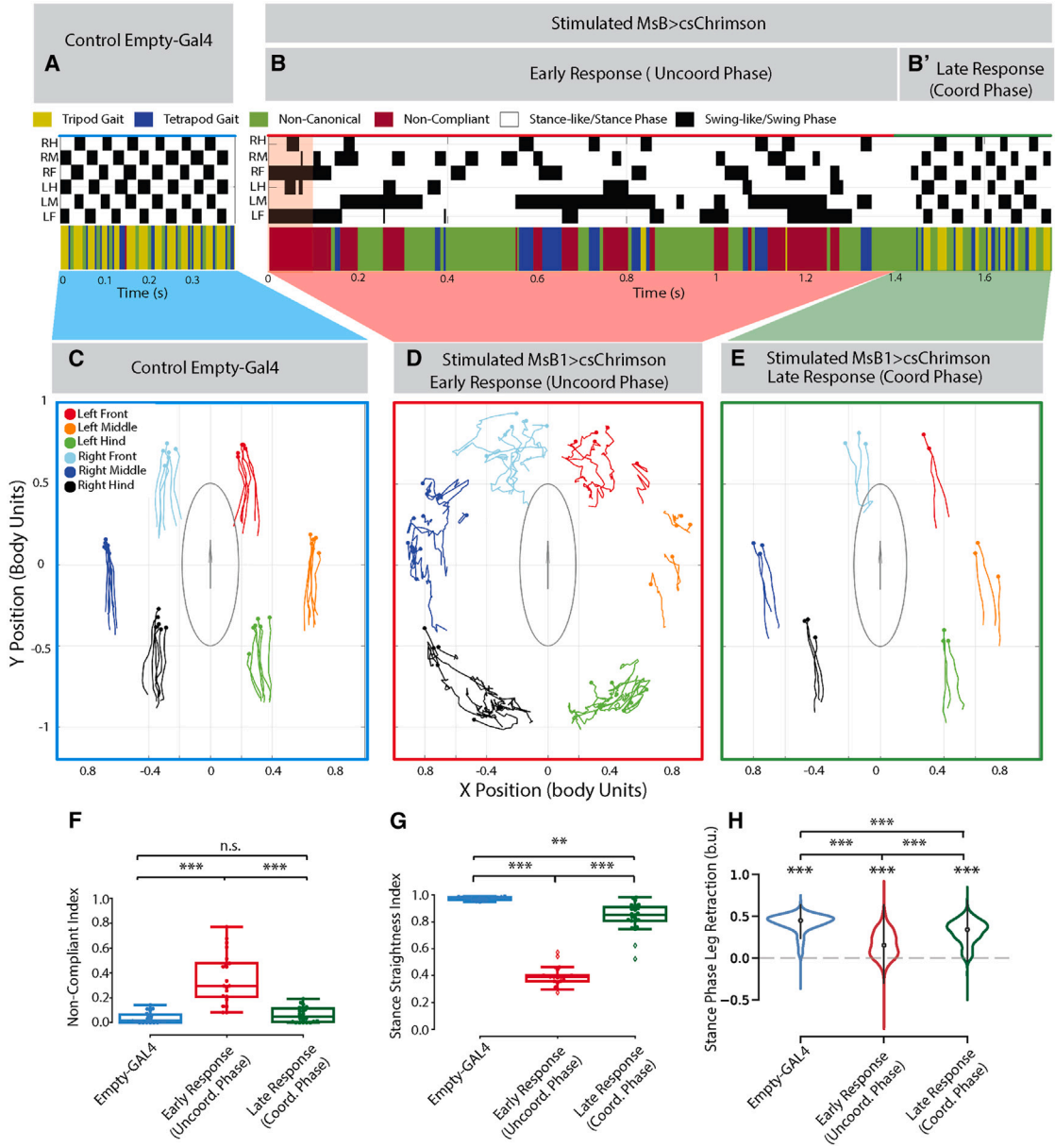

Figure 3. Kinematic analysis of walking patterns after MsB1 stimulation

(A and B) Representative gait features of MsB-evoked movement. The upper panel shows the flies' step patterns across time. For each leg, swing phases are represented in black and stance phases in white. For the uncoordinated phase, we describe each step as swing-like and stance-like. Right hind (RH), right middle (RM), right front (RF), left hind (LH), left middle (LM), and left front (LF). The lower panel represents the gaits adopted by the fly. For each frame, the corresponding gait was color coded as follows: yellow (tripod), blue (tetrapod), green (non-canonical), and red (non-compliant configuration; STAR Methods). 100 ms optogenetic stimulation is represented by a red shadow.

(A) Empty-GAL4 control (genotype: empty-GAL4, dac^{RE}-flp, UAS-FRT-stop-FRT-Chrimson-mVenus).

(B) Post-stimulus response of MsB1 flies (genotype: R65D12-GAL4, dac^{RE}-flp, UAS-FRT-stop-FRT-Chrimson-mVenus). 100 ms optogenetic stimulation is represented by a red shadow. The sequence is divided into early response (uncoordinated phase) and late response (coordinated phase) (B and B′, respectively).

(C–E) Representative stance traces. Traces are generated by the position of the stance phase footprints relative to the body center (set at 0.0,0.0). For each leg, stance onset corresponds to the anterior extreme position (AEP) (colored circle), while stance offset is termed posterior extreme position (PEP). Experimental conditions are color matched with previous panels.

(C) Control empty-GAL4 flies.

(D) Post-stimulation of MsB1 flies, early response corresponding to the uncoordinated phase.

(E) Post-stimulation of MsB1 flies, late response corresponding to the coordinated phase.

(F–H) Kinematic quantification between the empty-GAL4 control ($n = 20$), the early ($n = 21$), and late response post stimulated ($n = 23$). (F) Non-compliant index and (G) stance straightness index.

(legend continued on next page)

Please cite this article in press as: Medeiros et al., Mechanosensory bristles mediate avoidance behavior by triggering sustained local motor activity in *Drosophila melanogaster*, Current Biology (2024), https://doi.org/10.1016/j.cub.2024.05.021

Kinematic features after leg MsB stimulation in headless flies

We next investigated the kinematic features of headless flies' movement upon leg MsB stimulation (Figure 4) using the FlyWalker system. Stimulated headless flies exhibit uncoordinated gait pattern and stance-like traces (Figures 4A and 4B), akin to intact flies' uncoordinated phase (Figure S3D), with indistinguishable stance straightness indices between the two conditions (Figure 4C; compare Figure 3D with Figure 4B). As in the head-intact condition, the absence of sufficient fly pad contacts was compensated for by contacts of ventral portions of the body and proximal tarsal segments (Figure S3C; data not shown). However, the uncoordinated movement in headless flies lasted longer than the uncoordinated phase in head-intact flies (Figure 4D), suggesting that descending circuits can mediate the transition to a coordinated walking pattern. To explore this further we compared the "early response" in head-intact animals to the headless flies' response. We noticed a higher non-compliance index in headless flies (Figure 4E) but a maintenance of leg retraction during step cycles (Figure 4F). We subjected the kinematic parameters to a principal component analysis (PCA), selecting the top 3 components that explained most variance. PC1 (50.2% explained variance) showed a statistical difference between headless animals and the uncoordinated phase in head-intact animals (Figures S3E and 4G′).

These data indicate that leg MsBs can trigger sustained cyclic motor activity using solely circuits within the VNC, albeit with severely impaired coordination between legs and leg segments. This cyclic activity is modulated and ultimately restrained by brain circuits and descending information.

Inter-joint coordination is partially disrupted after MsB stimulation

To further explore the uncoordinated locomotion following leg MsB stimulation, we examined intra-leg (or inter-joint) coordination, i.e., the correct modulation of joint angles within a single limb in relation to another.[49] To visualize joint angles, we tethered flies expressing CsChrimson in leg MsBs to a wire while they freely gripped a polystyrene ball[50] (Figure 5A). One 100-ms light stimulation pulse was delivered while the flies were immobile and behavior was imaged using a lateral camera. Tracking by DeepLabCut[51] allowed the extraction of 3 joint angles: (1) coxa-femur joint, (2) femur-tibia joint, and (3) tibia-tarsus joint (Figures 5A, S4A, and S4B; Video S4). MsB stimulation induced leg movement in both head-intact and headless flies (Figure S4A; Video S4). To determine whether inter-joint coordination was perturbed by the stimulation protocol, we compared four conditions that capture the uncoordinated and coordinated phases of post-stimulation movement (Figures 3 and 4): walking flies (pre-stimulation) (Figure S4A, blue section), head-intact flies for the initial 1 s after stimulation onset (termed early response) (Figure S4A, red section), head-intact flies 3–5 s after stimulation onset (termed late response) (Figure S4A, green section), and headless flies for the first 1 s after stimulation onset (termed headless response) (Figure S4A, purple section).

As expected, pre-stimulation walking flies showed stereotyped periodic patterns of joint angles (Figure S4A).[53] We restricted our subsequent analysis to only coxa-femur and femur-tibia joints because these were strongly modulated throughout the step cycle in a correlated fashion (Figures S4A and S4B).

We performed fast Fourier transform (FFT) to extract component frequencies from data (Figures 5B and S4B). During pre-stimulation, coxa-femur and femur-tibia joints had highest power at 7.0 Hz, corresponding to the average step frequency (Figure S4B). In the intact-early response, the periodic modulation of joint angles was lost, but by late response a lower-frequency peak re-emerged (around 5.2 Hz). Strikingly, headless flies exhibit highly variable frequencies with no clear peaks (Figure 5B).

To further investigate the relationship between joints, we generated angle-angle plots between the coxa-femur joint and the femur-tibia joint for our 4 conditions (Figure 5C). Walking flies showed a half-moon-shaped "ring" trajectory (Figure 5C, pre-stim.) corresponding to the stance and swing phases of the step cycle. After stimulation, angle correlations were disturbed in the early response; transitioning to a consistent "walking-like" pattern in the late response (Figure 5C, early and late response). During headless response conditions, very distorted angle-angle traces are visible without a detectable ring pattern (Figure 5C, headless response). To quantify dispersion from the average walking cycle, we calculated the mean trace of the walking angles (black line in Figures 5C and S4C), and analyzed the minimum distance for each measured point to the mean trace (Figures 5D and 5E). Distances were reduced from the early response to the late response, while in the headless condition distances were greatly increased (Figure 5E). To identify disruptions in the angle-angle relationships, we divided the space into four quadrants based on stance and swing phases (Figure S4D). Headless flies exhibited a notable over-representation of points in quadrant 4 (Figure S4E), indicating extended femur-tibia angles. This tendency led to headless flies dropping the ball after stimulation (Video S4).

These data show that inter-joint coordination is partially lost immediately after stimulation in head-intact flies or in headless flies, suggesting a role for descending control to appropriately regulate the coordination between joint angles.

Intra-joint muscle coordination is maintained during movement triggered by MsB

Key for coherent locomotor activity is the reciprocal inhibition of opposing flexor and extensor muscles,[54] meaning that contraction

(H) Stance phase leg retraction for empty-GAL4 control (n = 650 steps) and the early (n = 697 steps) and late response post stimulated (n = 714 steps; STAR Methods). In (F) and (G), boxplots represent the median as the middle line, with the lower and upper edges of the boxes representing the 25% and 75% quartiles, respectively. Whiskers represent the range of the full dataset, excluding outliers represented by diamonds. Filled dots represent individual flies. Values are normalized for body size. Statistical analysis with Kruskal-Wallis ANOVA followed by Dunn's post hoc analysis, $^{**}p < 0.01$, $^{***}p < 0.001$. In (H), violin plots depict the distribution of stance phase leg retraction for each step, where the midpoint denotes the median value. Wilcoxon rank-test was employed to test whether values were different from 0. $^{***}p < 0.00$. Statistical analysis between groups with Kruskal-Wallis ANOVA followed by Dunn's post hoc analysis: $^{***}p < 0.001$. See also Figure S3 and Video S3.

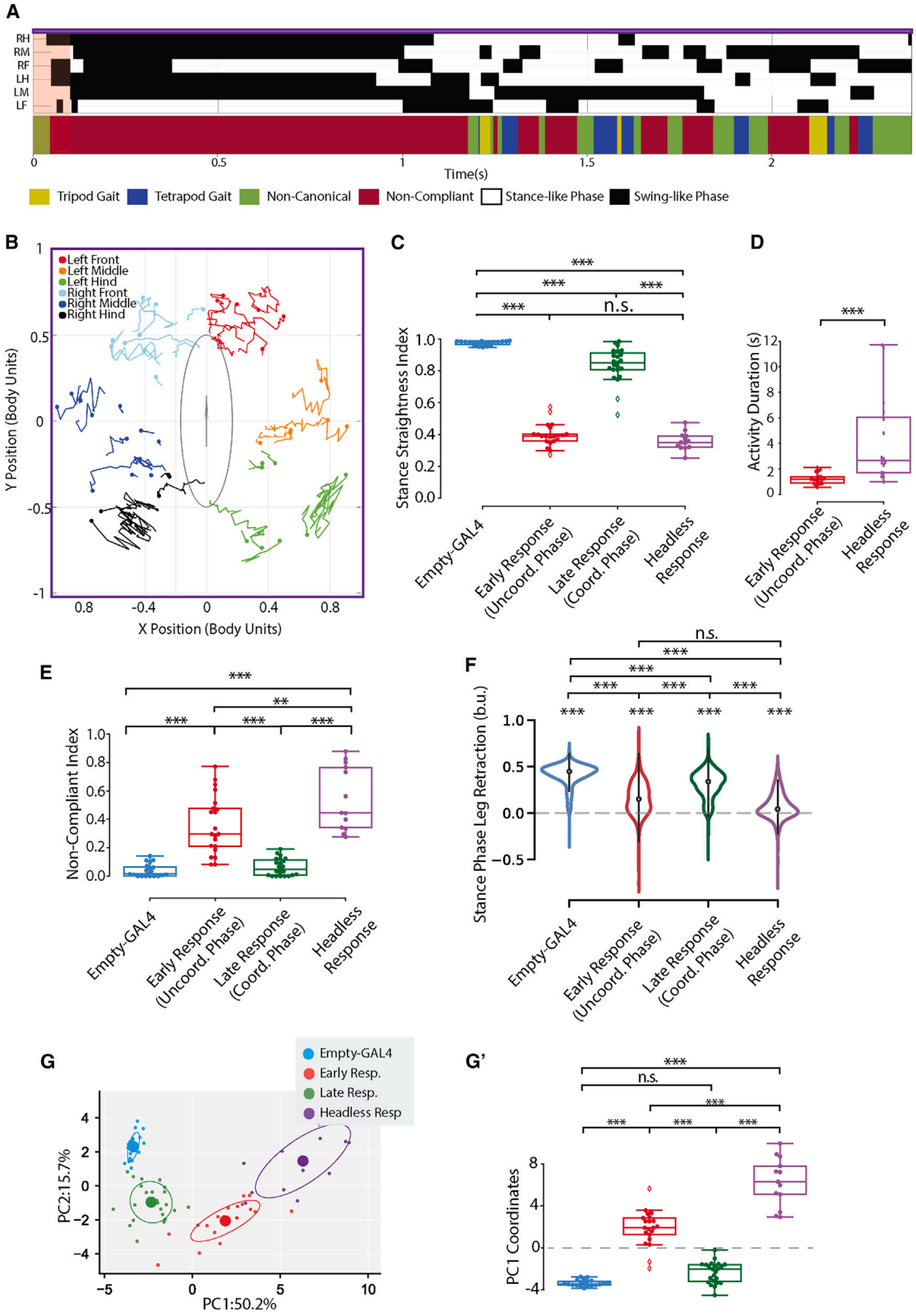

Figure 4. Mechanosensory-bristle-evoked movement is independent of the central brain

(A) Representative gait features after MsB stimulation of headless flies. Genotype: R65D12-GAL4, dac^{RE}-flp, UAS-FRT-stop-FRT-Chrimson-mVenus. The upper panel shows the flies' step patterns across time. For each leg, swing-like phases are represented in black and stance-like phases in white. Right hind (RH); right

(legend continued on next page)

Please cite this article in press as: Medeiros et al., Mechanosensory bristles mediate avoidance behavior by triggering sustained local motor activity in *Drosophila melanogaster*, Current Biology (2024), https://doi.org/10.1016/j.cub.2024.05.021

of one joint muscle is concurrently matched by relaxation of its antagonistic muscle. Because we observed a loss of movement rhythmicity, we questioned whether sensory-triggered movement still follows this muscle pattern, which we refer to as intra-joint coordination, or whether, alternatively, there are moments of muscle co-contraction. We monitored muscle GCaMP fluorescence at the femur-tibia joint as a proxy for muscle contraction while optogenetically stimulating leg MsBs (Figures 5F–5J and S5; Video S4).[55,56] The fly's body and legs were glued to a coverslip, and muscle activity in the femur was recorded using spinning disc confocal microscopy, followed by quantification of fluorescence in tibia levator and depressor muscles (Figures 5G–5I, S5A, and S5B; STAR Methods).[55] Optogenetic stimulation of leg MsBs showed a fast muscle response, maintaining an antagonistic alternation (Figures 5H and S5A; Video S5). Stimulation of MsBs in headless flies also led to alternating antagonistic muscle activity, albeit with a higher variability (Figures 5I and S5B; Video S5). Spearman correlations between the two muscle signals over time were negative, confirming their anti-phasic relationship (Figure 5E). In addition, by measuring the peak intensities and widths of the GCaMP fluorescence profile during muscle contraction (Figure S5C), we found that stimulation of leg MsBs in headless flies led to a weaker muscle contraction pattern compared with head-intact conditions (Figure S5D). Finally, as a proxy for co-contraction, we calculated the percentage of overlap between the two fluorescence curves using different thresholds (Figure S5F). We found a reduced percentage (below 10%) of fluorescence overlap between antagonistic muscles, irrespective of the threshold level (Figure S5F). Overall, these findings show that leg-MsB-stimulation-evoked movement largely maintains intra-joint muscle coordination properties in head-intact and headless flies.

MsBs evoke VNC-dependent avoidance behavior

Previous studies have highlighted the ability of MsBs to mediate avoidance behaviors in the context of inter-fly interactions or optogenetic stimulation of bristle neurons in the body.[19,57] Moreover, we confirmed that leg MsBs express DmPiezo-GAL4 (an excitatory channel component that mediates noxious mechanical stimuli[58]) (Figure S6). We then tested whether activating our leg-MsB line is sufficient to generate an aversive response, as previously reported.[19] We used a stadium-shaped behavioral chamber delimited by a red laser in the central region so that optogenetic activation would occur whenever flies crossed it (Figure 6A). Animals expressing CsChrimson under the control of MsB, ChO, or empty-GAL4 drivers were individually placed on side A of the chamber and their location tracked for 3 min (Figure 6A). Control animals and the ChO group showed equal occupancy of the two sides of the chamber (Figures 6A and 6B). In contrast, we found that animals expressing CsChrimson in leg MsBs displayed a strong avoidance behavior to the red laser, remaining almost exclusively on side A (Figure 6A and 6B). Next, we asked whether the interaction angle with the laser influences the avoidance response by comparing the angles at which flies approached the laser with the angular velocity, angle, and speed as flies moved away from it (Figure 6C; STAR Methods). We normalized the entry speed to 0° to 90°, as we observed no laterality bias when flies contacted the laser. We found that flies mostly react to laser contact by moving backward at angles similar to their entry (Figure 6D), particularly when flies entered with angles above 70° (almost perpendicular to the laser axis) (Figure 6D). Backward speed was inversely correlated with the entry angle (Figure 6E), with frontal entries (i.e., nearly perpendicular) showing faster retreat speeds (expressed in increased negative values). Flies also showed a concurrent rotational component as they exit away from the laser, measured by their angular speed (Figure 6F; data not shown), although we found no statistical bias with perpendicular entries (Figure 6F). These data suggest that flies integrate the directionality in which they encounter the stimulus and perform an appropriate avoidance response away from it, with the strongest response to a head-on stimulus.

Because other MsB lines with sparse expression patterns also showed a response to optogenetic stimulation in an open arena (Figure S2), we decided to test whether activation of smaller groups of cells could also mediate avoidance (MsB4, MsB5, MsB6, and MsB7) (Figure S2). By measuring the occupancy

middle (RM); right front (RF); left hind (LH); left middle (LM); left front (LF). The lower panel represents the gaits adopted by the fly. For each frame, the corresponding gait was color coded as follows: yellow (tripod), blue (tetrapod), green (non-canonical), and red (non-compliant configurations). 100 ms optogenetic stimulation is represented by a red shadow.

(B) Representative stance traces following optogenetic stimulation. Traces are generated by the position of the stance phase footprints relative to the body center (set at 0.0,0.0). For each leg, stance onset corresponds to the anterior extreme position (AEP) (colored circle) while stance offset is termed posterior extreme position (PEP).

(C) Stance straightness index in head-intact empty-GAL4 control ($n = 20$), early and late response ($n = 21$) of post-stimulated head-intact animals ($n = 23$), and post-stimulated headless flies ($n = 13$).

(D) Post-stimulation activity between head-intact (early response) and headless flies.

(E) Non-compliant index in head-intact empty-GAL4 controls, early and late response of post-stimulated head-intact animals, and post-stimulated headless flies.

(F) Violin plots depicting the distribution of stance phase leg retraction for each step for empty-GAL4 controls ($n = 650$ steps), early ($n = 697$ steps), late response of post-stimulated head-intact animals ($n = 714$ steps), and post-stimulated headless flies ($n = 386$ steps). The midpoint denotes the median value. Wilcoxon rank-test was employed to test whether values were different from 0. $^{***}p < 0.001$. Statistical analysis between groups with Kruskal-Wallis ANOVA followed by Dunn's post hoc analysis: $^{*}p < 0.05$; $^{**}p < 0.01$; $^{***}p < 0.001$.

(G and G′) PCA of all kinematic parameters in head-intact empty-GAL4 controls, early and late response of post-stimulated head-intact animals, and post-stimulated headless flies. (G) Two-dimensional (2D) representation of PC1-PC2 with ellipses delimiting 50% of variance of the data. (G′) Comparison of each PC1 coordinates.

In (C)–(E) and (G′), boxplots represent the median as the middle line, with the lower and upper edges of the boxes representing the 25% and 75% quartiles, respectively, whiskers represent the range of the full dataset, excluding outliers represented by diamonds. Filled dots represent individual flies. Values are normalized for body size. Statistical analysis with Kruskal-Wallis ANOVA followed by Dunn's post hoc analysis: $^{*}p < 0.05$; $^{**}p < 0.01$; $^{***}p < 0.001$. See STAR Methods for details.

See also Figure S3 and Video S3.

Please cite this article in press as: Medeiros et al., Mechanosensory bristles mediate avoidance behavior by triggering sustained local motor activity in *Drosophila melanogaster*, Current Biology (2024), https://doi.org/10.1016/j.cub.2024.05.021

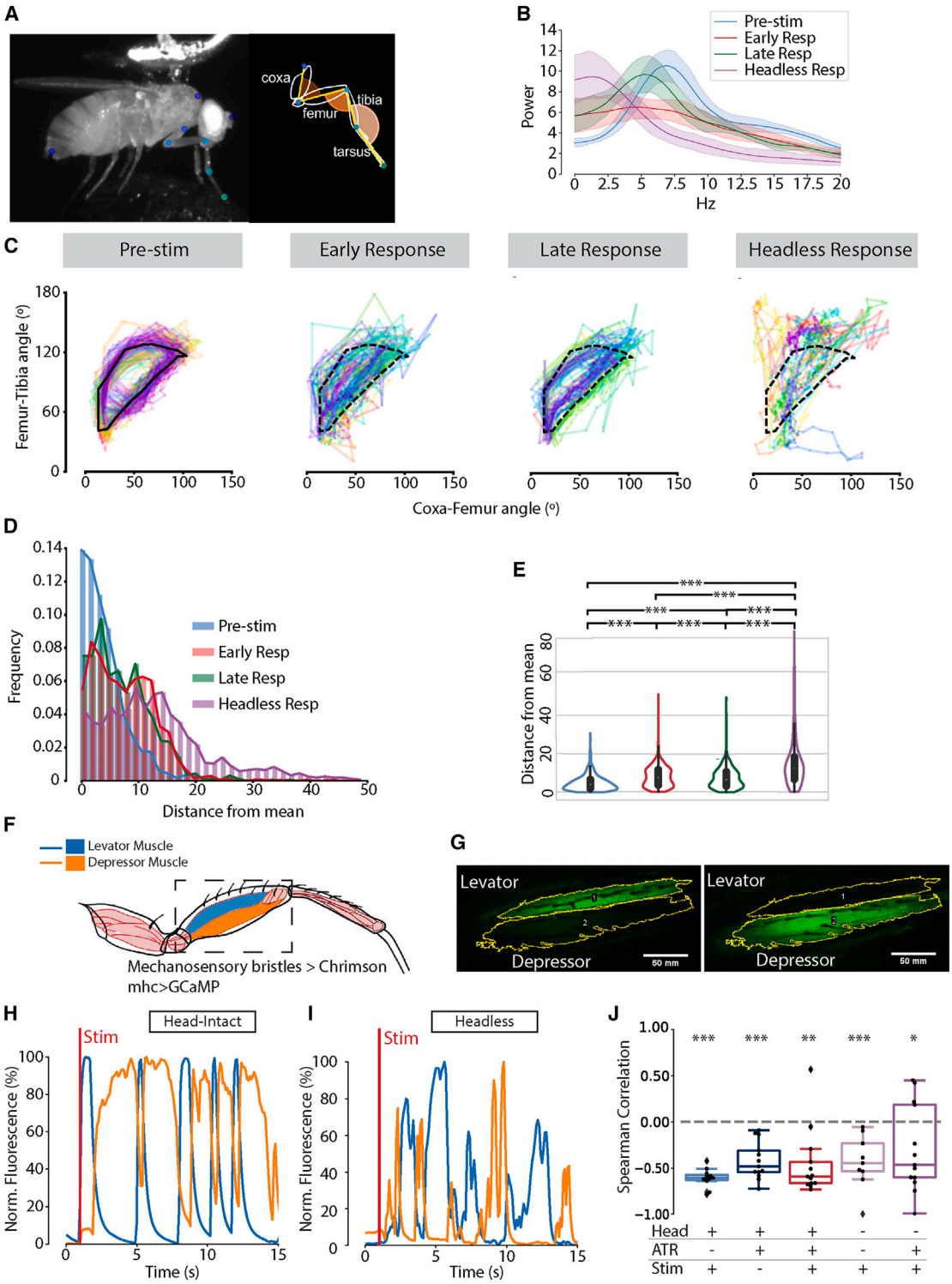

Figure 5. Mechanosensory-bristle-evoked movement shows partially disrupted inter-joint coordination but muscle activity alternation is maintained

(A) Tethered fly setup showing tracked joint positions (blue/green circles). Insect schematic of fly T1 leg showing 5 segments and 3 measured joint angles (brown, coxa-femur angle; bright orange, femur-tibia angle; light orange, tibia-tarsus angle). For simplicity, the fused trochanter-femur joint is included in the coxa-femur joint. Conditions were head-intact early response (n = 11), head-intact late response (n = 6), and headless response (n = 7).

(B) Fast Fourier transform of leg angles for the coxa-femur joint.

(legend continued on next page)

Please cite this article in press as: Medeiros et al., Mechanosensory bristles mediate avoidance behavior by triggering sustained local motor activity in *Drosophila melanogaster*, Current Biology (2024), https://doi.org/10.1016/j.cub.2024.05.021

density for each genotype, we noticed that flies with sparse labeling showed a variable avoidance profile, which was less extreme than MsB1 (Figure 6G). Initially, we assessed the frequency of fly crossings of the high-intensity laser zone, normalized to their average walking speed (STAR Methods). Consistent with earlier results, the control group showed many crossings, whereas MsB1 displayed a clear avoidance behavior, with only a single cross observed in all the flies tested (Figure 6H). MsB4 and MsB5 showed a significant reduction in crossings compared with the control, while MsB6 and MsB7 did not show a change in crossing number, although a change in behavior was visible while crossing the laser area (e.g., Figure 6L; data not shown). Upon close video inspection, we observed a noticeable hesitation among flies in groups MsB1, MsB4, and MsB5 as they approached the high-intensity laser zone's edge. We defined a peri-laser zone (gray section in Figure 6G) to capture this area of the arena and calculated fly speeds and time spent within this area. We found a significant increase in time spent in the peri-laser zone for the groups MsB1, 4, and 5 when compared with the control group (Figure 6I). To assess the extent of laser avoidance, we analyzed the percentage of time spent within the high-intensity laser zone (red section in Figure 6G). Surprisingly, while MsB1 lines showed an almost complete avoidance of the high-intensity zone, MsB4, and to some extent MsB5, spent an increased amount of time there as compared with the control (Figure 6J). Given the previously described role of MsBs in inducing grooming behavior,[16] we quantified the percentage of time flies spent grooming in this area and, indeed, MsB4 and MsB5 showed a significant increase (Figure 6K), thus explaining the increased occupancy. It should be noted that some leaky off-target labeling of the GAL4 drivers was observed in the optic lobes of MsB4 and MsB5 (Figure S6B). However, the avoidance response in these lines resembles the full MsB line, and increased grooming in the laser area suggests that MsBs drive the response, not off-target cells. To understand the frequencies of behaviors after laser touch, we categorized the post-laser interaction behavior into 4 classes: move away from the laser after contact, stay in the peri-laser zone, stay in the laser zone, or cross (Figures 6L and 6M; STAR Methods). We found that the MsB1 flies tend to have a higher percentage of move away events when compared with the other MsB lines. Moreover, the responses from both lines, MsB4 and MsB5, exhibited high percentages of laser avoidance but predominantly remained in the peri-laser zone with few move away responses (Figure 6M). Curiously, the MsB7 line exhibited some instances of moving away from the laser. Nonetheless, in general, the responses of MsB6 and MsB7 showed limited avoidance, mostly crossing the laser area (Figure 6M; data not shown).

These data suggest that MsBs mediate avoidance responses depending on the number of bristles engaged. While engagement of more bristles leads to total avoidance of the area and moving away from the area of stimulation, engagement of fewer bristles leads to grooming, a behavior used to avoid and remove contact of dust or parasites.

The direction of the response triggered by MsBs can be mediated by the VNC

An avoidance response involves moving away from an unwanted stimulus, requiring a choice of directional movement. We therefore asked whether targeted stimulation of fore- or hindleg MsBs in immobile animals could elicit a motor avoidance behavior similar to extreme temperatures or noxious odors.[59] For this, we performed targeted laser stimulation of fore or hind legs on immobile animals expressing CsChrimson in leg MsBs (Figure 7A). We found that flies move away from the source of the stimulus immediately after being stimulated (Figures 7A′ and 7A″; Video S6). We next asked whether the response to targeted stimulation of leg MsBs was independent of brain circuits. Remarkably, we found the same directionality of movement in headless animals, with animals moving away from the stimulation site (Figures 7B and 7B″), although the distance traveled was considerably reduced.

We then tested whether the kinematic response to targeted stimulation of leg MsBs was comparable to stimulation of all

(C) Angle-angle plots of coxa-femur versus femur-tibia angles over time. Different colors represent individual trials. Black line and dotted lines indicate the mean trace of the walking condition over the step cycle.

(D) Histogram representing the distribution of distances between individual points and the mean walking trace.

(E) Violin plots depicting the distribution of distances between individual points and the mean walking trace. Distances were significantly increased for all stimulated conditions as compared with pre-stimulus condition, indicating a significant disruption of the coordination between joints after MsB stimulation ($p_{\text{walking-early response}} < 0.001$, $p_{\text{walking-late response}} < 0.001$, $p_{\text{walking-decapitated}} < 0.001$, Dunn's test) Distances were reduced from the early response to the late response, indicating a partial recovery of coordination ($p_{\text{early response-late response}} < 0.001$, Dunn's test). In contrast, distances were greatly increased in the headless condition, indicating that loss of brain control leads to wildly disrupted relationships between joint angles ($p_{\text{early response-decapitated}} < 0.001$, $p_{\text{late response-decapitated}} < 0.001$, Dunn's test). p values were calculated using Dunn's post hoc test. ***$p < 0.001$.

(F) Leg schematic showing tibia levator (blue) and depressor (orange) muscles in the femur. Adapted from Venkatasubramanian et al.[52] Dashed rectangle represents the scanned region of the genotype: lexO-GCaMP6f; mhc-lexA:LHV2, dac^{RE}-flp;UAS-FRT-stop-FRT-CsChrimson-mVenus, R65D12-GAL4.

(G) Representative images of a femur showing levator (top) or depressor muscles (lower) contraction, resulting in GCaMP fluorescence inside the respective muscles. Yellow lines depict the regions of interest (ROIs) used for fluorescence calculations.

(H and I) Representative plots showing the fluctuation of fluorescence for levator (blue) and depressor (orange) muscles across time. Red bar represents the 100-ms red light stimulation. Values are normalized to the maximum signal measured in each ROI throughout the experiment, corresponding to 100%. (H) Head-intact flies ($n = 13$); (I) headless flies ($n = 13$).

(J) Spearman correlation analysis between levator and depressor muscles activity across different experimental conditions. A positive Spearman correlation signifies synchronous or in-phase muscle activity; conversely, negative values indicate an out-of-phase or antagonistic relationship between the muscles. Boxplots represent the median as the middle line, with the lower and upper edges of the boxes representing the 25% and 75% quartiles, respectively. Whiskers represent the range of the full dataset, excluding outliers represented by diamonds. Filled dots represent individual flies. Statistical analysis with Kruskal-Wallis ANOVA followed by Dunn's post hoc analysis revealed no significant difference between the groups. Wilcoxon test was employed to test whether correlations were different from zero; all groups showed a significant negative correlation.

See also Figures S4 and S5 and Videos S4 and S5.

Please cite this article in press as: Medeiros et al., Mechanosensory bristles mediate avoidance behavior by triggering sustained local motor activity in *Drosophila melanogaster*, Current Biology (2024), https://doi.org/10.1016/j.cub.2024.05.021

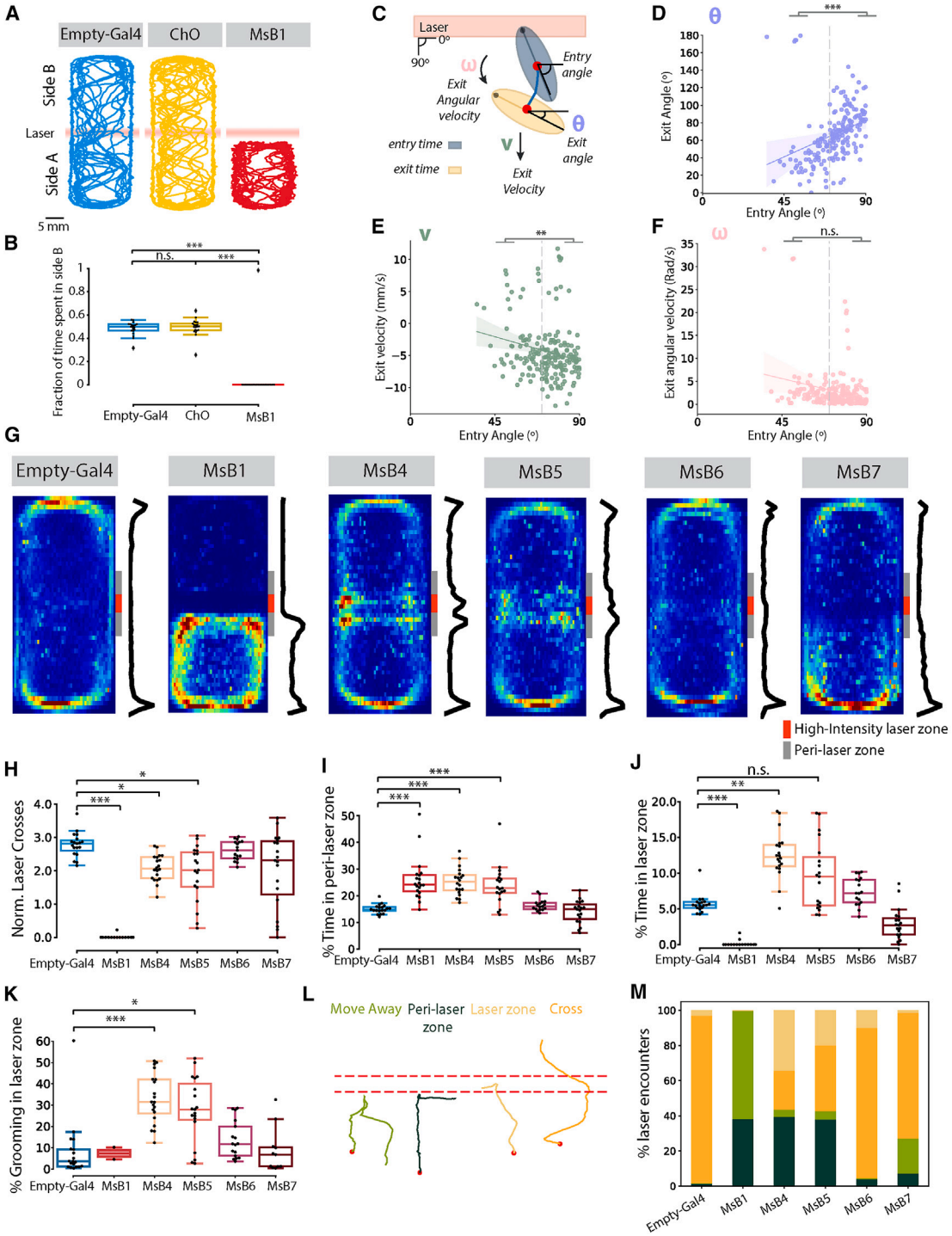

Figure 6. Stimulation of leg mechanosensory bristles elicits an avoidance response

(A) Representative trajectories of freely moving flies in an arena crossed in the middle by a laser beam (red bar). Empty-GAL4 (blue), ChO (yellow), and MsB (red).

(B) Proportion of time spent on side B of the arena per condition ($n = 20$, for all conditions). Arena is divided by the laser line; side B is the side opposite to which the flies started.

(C) Schematic illustrating trajectories of flies following laser interaction, as well as the measurements of angles (exit and entry, θ), velocity (v), and angular velocity (ω). Two different time points are depicted (entry time: moment of contact with the laser; exit time: 5 frames after laser interaction. Entry angles were adjusted to fall within the range of 0° and 90° (STAR Methods). We excluded from this analysis events in which the fly stayed around the peri-laser area (<40%).

(legend continued on next page)

Please cite this article in press as: Medeiros et al., Mechanosensory bristles mediate avoidance behavior by triggering sustained local motor activity in *Drosophila melanogaster*, Current Biology (2024), https://doi.org/10.1016/j.cub.2024.05.021

legs (Figure 3). Indeed, we found that after hindleg stimulation, head-intact flies display an initial uncoordinated phase followed by a coordinated phase (Figure 7C; compare to (Figure 3B). Moreover, the uncoordinated phase showed a high fraction of non-compliant configurations at levels similar to those seen in the uncoordinated phase of stimulation of all legs (Figure 7D). Notably, during front stimulation, backward walking only showed an apparent uncoordinated pattern, as afterward animals turned away from the stimulus source and walked forward (data not shown). Additionally, back stimulation led to a stance-like phase largely associated with leg retraction (Figure 7E), while front stimulation led to reversal of this configuration, with stance-like phase bouts largely associated with leg protraction (represented as negative values in Figure 7E), leading a backward motion of the body.

We next employed the tethered fly setup to probe whether decapitated flies were able to achieve directionality by engaging in functional step cycles when stimulated from one end only. As with the open-field setup, decapitated flies reacted in a directional manner to the stimulation. In particular, front stimulation was very effective at driving backward movement on the ball, while back stimulation was less efficient, with flies showing less directionality (Figure 7F). Interestingly, decapitated flies exhibited the ability to execute backward step cycles upon receiving front stimulation, notably evident in the T3 leg, reversing the typical joint angle adjustments observed during forward locomotion. (Figure 7G, upper section, compare with lower section; Video S6). A similar process has been observed in backward walking elicited by the moonwalker descending neurons.[53]

Overall, these results suggest that leg MsBs can mediate mechanical aversive behaviors and that the motor directionality generated by these exteroceptors is at least partially encoded within the fly's VNC.

DISCUSSION

In this study, we unveil a new parallel circuit for direct activation of VNC locomotor neural networks resulting in a fast, sustained directional motion. Previous studies in *Drosophila* have shown that stimulation of mechanosensory structures initiates behavioral programs such as grooming[60] or backleg kicks to remove invading mites,[15] which can be executed by VNC circuits with remarkable speed and precision. Our data show that neural networks in the VNC can process leg mechanosensory feedback to execute a distinct cyclic motor program, driving body displacement. Notably, the location of the sensory input largely determines the motor outcome rather than solely the class of the mechanosensory structures stimulated (Figure 2).[15] Because the leg and wing MsBs target distinct neuropil regions in the VNC[14] (Figure S1), it is likely that distinct motor circuits become active.

While grooming and kicking after bristle stimulation help the fly to rid itself of parasites and debris, the uncoordinated forward movement here does not follow the same purpose. Instead, our data highlight the role of leg MsBs as mediators of mechanical aversive stimuli, leading to an avoidance response caused by inter-fly contacts or other physical imminent threats (Figures 6 and 7).[57] This response can also be seen in an innate motor reflex termed startle-induced locomotion.[61,62] Interestingly, in a screen for modifiers of this behavior, Yamamoto and colleagues identified several genes that regulate MsB number and neuronal terminal differentiation.[62,63] Accordingly, our data suggest MsBs can elicit a rapid motor response to mechanically induced, potentially dangerous situations at the expense of a coordinated, albeit slower, response, which could be mediated by DNs. Consistently, we found a strikingly faster response upon stimulation of MsBs compared with ChO (Figure 1D). This strategy resembles the fast jump response to escape from a predator attack. In this response, stability is traded off for speed, contrasting with an alternative slow and coordinated take-off jump.[64,65] Another aversive behavior can be found in the zebrafish, where the intensity of sensory stimulation can also impact the latency of the escape response, wherein stronger stimulation results in a shorter latency response.[66] These avoidance behaviors display a directionality component away from the place where the avoidance stimulus originates, which requires descending control to permit postural adjustments.[19,57,65,67] In mammals, spinal withdrawal reflexes can occur in millisecond timescales,[68] which can nevertheless be sensitized (i.e., facilitated or inhibited) by descending commands.[69] While the descending commands that govern oriented walking avoidance are only partly understood,[40,70] our data suggest that circuits within the VNC mediate part of the directionality component of the motor response (Figure 7). In the stick insect, load sensors drive a

(D–F) Plots showing the correlation between the entry angle and various parameters, such as (D) exit angle, (E) exit velocity, and (F) exit angular velocity. The line represents the regression fit and the shadow the confidence interval. The Pearson correlation coefficients are the following: entry angle versus exit angle (0.32); entry angle vesus exit velocity (−0.2); entry angle versus exit angular speed (−0.23) (n = 194 contact events).
(G) Density plots showing the frequency of distribution of occupation the arena. Warmer colors indicate a higher density for all conditions (n = 17∼21). The red bar indicates the high-intensity laser zone, while the gray bar indicates the peri-laser zone.
(H) Number of high-intensity laser area crosses normalized to speed.
(I) Percentage of time spent in peri-laser zone. Area surrounding the laser, 4.8 mm for each side: starting at 0.2 mm from the edge of the laser.
(J) Percentage of time spent inside the high-intensity laser zone.
(K) Percentage of grooming inside the laser zone.
(L) Example traces of instances of contact with the laser. Classification of interaction with the laser: move away, light green; peri-laser zone, dark green; laser zone, yellow; cross, orange (STAR Methods). Red dotted line represents the high-intensity laser zone.
(M) Plot representing the percentage of laser encounters for each category.
(B and H–K) Boxplots represent the median as the middle line, with the lower and upper edges of the boxes representing the 25% and 75% quartiles, respectively. Whiskers represent the range of the full dataset, excluding outliers represented by diamonds. Filled dots represent individual flies. Statistical analysis with Kruskal-Wallis ANOVA followed by Dunn's post hoc analysis. (D–F) Statistical analysis with t test. *$p < 0.05$; **$p < 0.01$; ***$p < 0.001$. See STAR Methods for details. See also Figure S6.

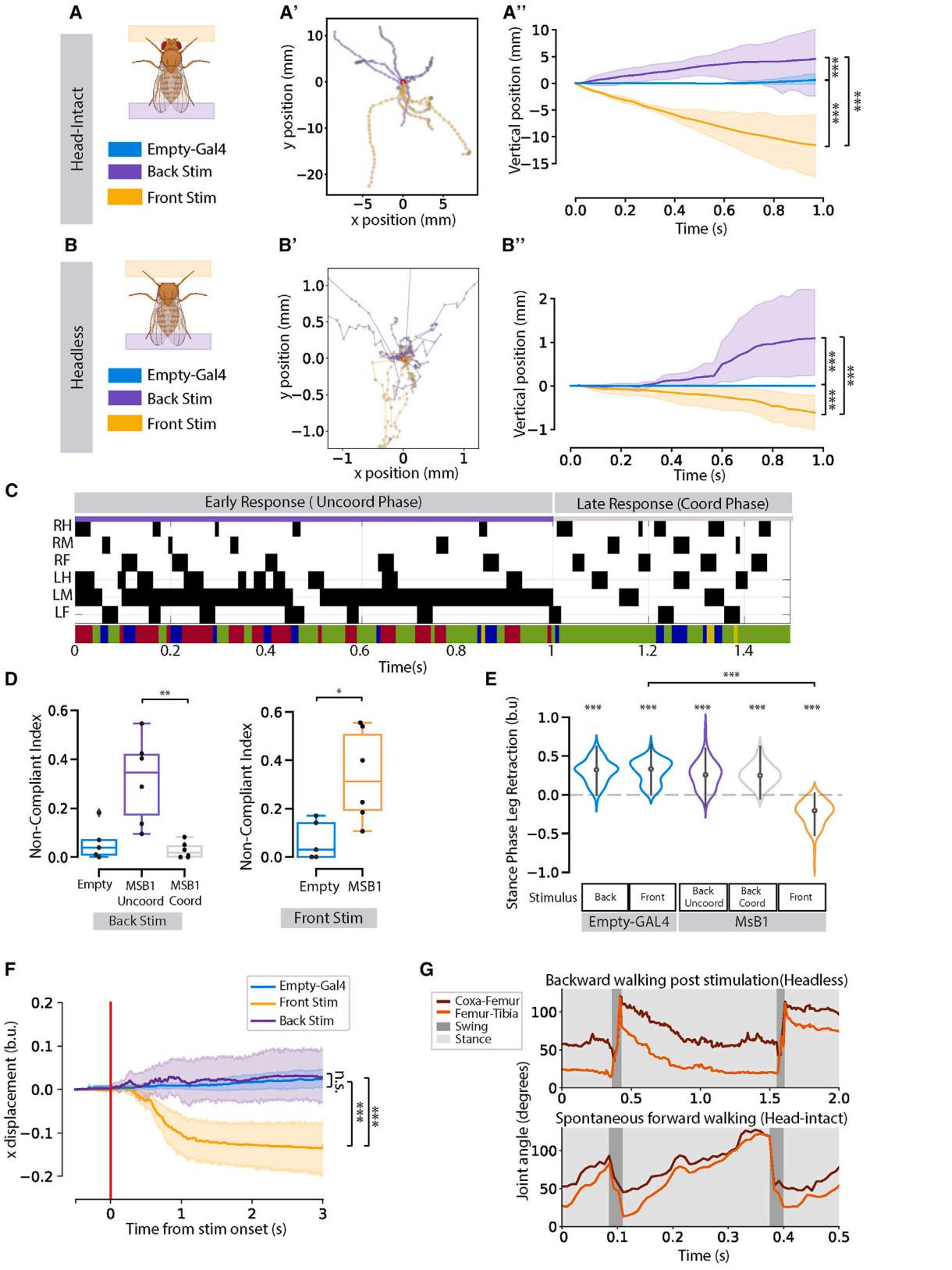

(legend on next page)

Please cite this article in press as: Medeiros et al., Mechanosensory bristles mediate avoidance behavior by triggering sustained local motor activity in *Drosophila melanogaster*, Current Biology (2024), https://doi.org/10.1016/j.cub.2024.05.021

reversal of CPG outputs—possibly via inhibitory circuits—so that protractor muscles contract during the stance phase while retractor muscles do so during the swing phase of the stepping cycle, leading to backward walking.[71–73]

Based on our data, we propose a model in which stimulation of leg MsBs specifically activates VNC circuits in the leg neuropil that lead to a fast but uncoordinated motor output (Figure S7, blue circuit). In parallel, the activity of MsBs or other proprioceptive structures perceive leg movements and relay this information via ascending neurons to higher-order centers that inhibit uncoordinated movements and trigger coordinated motor output via DNs (Figure S7, orange circuit). In this study, the movement evoked by the stimulation of MsBs shows characteristic CPG-like activation, during which antagonistic muscles maintain anti-phasic contraction leading to joint movement (Figure 5).[74–76] The same behavior was observed in headless flies, implying a lack of interference of ascending or descending neurons in the sensory-evoked movement. These results resemble pharmacological stimulation of decapitated flies with stimulatory amines, which leads to locomotor bouts.[77] Moreover, studies in deafferented VNCs, using the muscarinic cholinergic agonist pilocarpine, have shown alternating and rhythmic activity in antagonistic leg motor neuron pools driven by the CPGs.[75,76,78,79] Despite extensive research, the identity, location, and architecture of the CPG population remain largely unknown due to challenges in accessing neuronal VNC populations. Nevertheless, certain interneurons have been identified within this network in both cockroaches and stick insects.[76,80] Alternatively, the MsB-induced motor activity could be the product of a feedback loop between leg sensory afferents and local VNC circuits driving the motor oscillation. Such a closed-loop model has been described for the stick insect[81–83] and *C. elegans*.[84] The reconstruction of the *Drosophila* VNC using serial-section electron microscopy (EM) datasets in combination with the expanding *Drosophila* genetic toolkit will contribute to establishing the functional connectivity of the leg MsBs.[85]

Remarkably, we found reduced intersegmental coordination between hemisegments and leg joints immediately after MsB stimulation (Figures 3, 4, and 5), albeit with antagonistic muscle contraction still being maintained (Figure 5). Moreover, this rhythmic activity is independent within the three leg joints, as these rarely exhibit coordinated activity between one another, meaning that different CPGs control the antagonistic activity of motor neuron pools of each leg joint.[76] Given that in our experimental design, animals still maintain their proprioceptive structures that assist in segment coupling, we can speculate that MsB-dependent cyclic activity overrides or is insensitive to sensory feedback or to any other coupling mechanism. Our data also suggest a role for descending feedback promoting segmental coordination because decapitation decreased the degree of inter- and intra-leg coordination (Figures 4, 5, S3D, and S4). Work on hemimetabolous insects has shown a role for DNs controlling the onset and features of walking patterns, including reverse walking.[7,86,87] Moreover, optogenetic manipulation of defined populations of DNs can trigger stereotyped behaviors and change walking patterns.[7,88] Multisegmental coupling is provided either by sensory feedback, descending inputs, or centrally by nonspiking interneurons,[76,89] with

Figure 7. Targeted stimulation of leg mechanosensory bristles reveals a directionality component of the avoidance response in head-intact and headless flies

(A) Schematic representation of laser beam activation of front (orange) and back (purple) legs in head-intact flies.

(A′) Trajectories of the fly after laser stimulation of the front and back legs for the groups empty-GAL4 front and back stimulation (blue, $n = 13$), back stimulation of MsB flies (purple, $n = 5$), and front stimulation of MsB flies (orange, $n = 5$). The red dot indicates the starting frame for all flies. Each gray dot represents one frame; 30 frames were considered.

(A″) Vertical positions after laser stimulation over time.

(B) Same as (A) in headless flies. Groups empty-GAL4 front and back stimulation (blue, $n = 10$), back stimulation of MsB flies (purple, $n = 10$), and front stimulation of MsB flies (orange, $n = 8$).

(B′) See (A′). 30 frames were considered.

(B″) See (A″).

(C) Representative gait features of an MsB1 head-intact fly after targeted laser stimulation of back legs. Genotype: R65D12-GAL4, dac^{RE}-flp, UAS-FRT-stop-FRT-Chrimson-mVenus. The upper panel shows the fly's step patterns across time. For each leg, swing phases are represented in black and stance phases in white. Right hind (RH); right mid (RM); right front (RF); left hind (LH); left middle (LM); left front (LF). The lower panel represents the gaits adopted by the fly. For each frame, the corresponding gait was color coded as follows: yellow (tripod), blue (tetrapod), green (non-canonical), and red (non-compliant configurations). The sequence is divided into an uncoordinated phase (purple) and a coordinated phase (gray).

(D) Non-compliant index in empty-GAL4 controls and uncoordinated and coordinated response of post-stimulated head-intact animals after targeted back stimulation and front stimulation.

(E) Violin plots depicting the distribution of stance phase leg retraction for each step for empty-GAL4 controls front ($n = 119$ steps) and back ($n = 121$ steps) stimulations, for MsB1 back stimulation: uncoordinated ($n = 121$) and coordinated response ($n = 121$ steps) and MsB1 front stimulation ($n = 76$ steps). The midpoint denotes the median value. Wilcoxon rank-test was employed to test whether values were different from 0. $^{***}p < 0.001$. Statistical analysis between groups with Kruskal-Wallis ANOVA followed by Dunn's post hoc analysis: $^{*}p < 0.05$; $^{**}p < 0.01$; $^{***}p < 0.001$. Each control was compared with the respective experimental group. No statistical significance was found between the conditions back stimulation control and the respective back stimulation groups.

(F) Fictive X displacement of the ball over time, indicative of the direction of the movement of the fly, for 3 headless conditions: empty-GAL4 flies pooled front and back stimulation (blue, $n = 12$ stimulations [4 flies]), MsB front stimulation (orange, $n = 17$ stimulations [6 flies]), and MsB back stimulation (purple, $n = 16$ stimulations [7 flies]).

(G) Modulation of coxa-femur and femur-tibia joint angles of the hind (T3) leg throughout time for MsB1 backward walking induced by front stimulation in headless flies (upper) and spontaneous forward walking in head-intact flies (lower). Dark gray and light gray represent swing and stance phases, respectively. Boxplots represent the median as the middle line, with the lower and upper edges of the boxes representing the 25% and 75% quartiles, respectively. Whiskers represent the range of the full dataset, excluding outliers represented by diamonds. Filled dots represent individual flies. Statistical analysis with Kruskal-Wallis ANOVA followed by Dunn's post hoc analysis: $^{*}p < 0.05$; $^{**}p < 0.01$; $^{***}p < 0.001$.

See also Video S6.

slow-walking animals—such as the stick insect—relying heavily on sensory feedback.[23,71,90] Our results suggest that, as in other insects, alternating activity of antagonistic motor pools in *Drosophila* are uncoupled between different joints and hemisegments, further reinforcing the use of this model system to unravel the neuronal architecture responsible for coordinated motor patterns.

STAR★METHODS

Detailed methods are provided in the online version of this paper and include the following:

- KEY RESOURCES TABLE
- RESOURCE AVAILABILITY
  - Lead contact
  - Materials availability
  - Data and code availability
- EXPERIMENTAL MODEL AND SUBJECT DETAILS
  - Fly stocks
- METHOD DETAILS
  - Behavior setup and optogenetic activation of mechanosensory structures
  - Video acquisition and Tracking
  - Behavioral classifiers
  - fTIR imaging and FlyWalker software
  - Tethered fly imaging
  - Leg and VNC dissection and Mounting
  - *In vivo* calcium imaging during leg stimulation
- QUANTIFICATION AND STATISTICAL ANALYSIS

SUPPLEMENTAL INFORMATION

Supplemental information can be found online at https://doi.org/10.1016/j.cub.2024.05.021.

ACKNOWLEDGMENTS

We thank the Mendes lab, Rita Teodoro, and her lab for comments and suggestions during the execution of this project; Allan Mancoo for feedback on data analysis; Inês Fernandes and Margarida Brotas for experimental assistance; Rita Fernandes for advice on Figure 5; Manuel Tanqueiro for setup assistance for Figure 6; and Luísa Vasconcelos, Turgay Akay, Daniela Pereira, Ana Rita Colaço, and Margarida Brotas for comments on the manuscript. We thank Mirian Zecca and Richard Mann for support generating the transgenic lines used in this study. We also thank CONGENTO consortium for genetically tractable organisms and the Fly Platform, the Scientific Hardware Platform at the Champalimaud Centre for the Unknown, and the Bloomington Drosophila Stock Center for fly stocks. This work was supported by Fundação para a Ciência e a Tecnologia (FCT) (PTDC/BIA-COM/0151/2020), iNOVA4Health (UIDB/04462/2020 and UIDP/04462/2020), and LS4FUTURE (LA/P/0087/2020) to C.S.M. A.M. was supported by a doctoral fellowship from FCT (PD/BD/128445/2017).

AUTHOR CONTRIBUTIONS

A.M.M., A.F.H., and C.S.M. contributed to conception and design of the study; A.M.M. performed the experiments and analyzed the raw data; A.F.H. performed data acquisition and analysis of Figures 5 and 7 and contributed to the analysis of Figures 5, 6, and 7 data; G.B. contributed to analysis of and data acquisition for Figure S2; and A.M.M., A.F.H., M.M., and C.S.M. wrote the manuscript. All authors contributed to manuscript revision and read and approved the submitted version.

DECLARATION OF INTERESTS

The authors declare no competing interests.

Received: June 21, 2023
Revised: March 12, 2024
Accepted: May 13, 2024
Published: June 10, 2024

REFERENCES

1. Dickinson, M.H., Farley, C.T., Full, R.J., Koehl, M.A., Kram, R., and Lehman, S. (2000). How animals move: an integrative view. Science *288*, 100–106. https://doi.org/10.1126/science.288.5463.100.
2. Alexander, R.M. (2003). Principles of Animal Locomotion, Student Edition (Princeton University Press).
3. Camhi, J.M., and Nolen, T.G. (1981). Properties of the escape system of cockroaches during walking. J. Comp. Physiol. *142*, 339–346. https://doi.org/10.1007/BF00605446.
4. Ritzmann, R.E., Pollack, A.J., Archinal, J., Ridgel, A.L., and Quinn, R.D. (2005). Descending control of body attitude in the cockroach Blaberus discoidalis and its role in incline climbing. J. Comp. Physiol. A Neuroethol. Sens. Neural Behav. Physiol. *191*, 253–264. https://doi.org/10.1007/s00359-004-0537-0.
5. Ritzmann, R.E., Harley, C.M., Daltorio, K.A., Tietz, B.R., Pollack, A.J., Bender, J.A., Guo, P., Horomanski, A.L., Kathman, N.D., Nieuwoudt, C., et al. (2012). Deciding which way to go: how do insects alter movements to negotiate barriers? Front. Neurosci. *6*, 97. https://doi.org/10.3389/fnins.2012.00097.
6. Robie, A.A., Hirokawa, J., Edwards, A.W., Umayam, L.A., Lee, A., Phillips, M.L., Card, G.M., Korff, W., Rubin, G.M., Simpson, J.H., et al. (2017). Mapping the neural substrates of behavior. Cell *170*, 393–406.e28. https://doi.org/10.1016/j.cell.2017.06.032.
7. Cande, J., Namiki, S., Qiu, J., Korff, W., Card, G.M., Shaevitz, J.W., Stern, D.L., and Berman, G.J. (2018). Optogenetic dissection of descending behavioral control in Drosophila. eLife *7*, e34275. https://doi.org/10.7554/eLife.34275.
8. Schnell, B., Ros, I.G., and Dickinson, M.H. (2017). A descending neuron correlated with the rapid steering maneuvers of flying Drosophila. Curr. Biol. *27*, 1200–1205. https://doi.org/10.1016/j.cub.2017.03.004.
9. Bidaye, S.S., Laturney, M., Chang, A.K., Liu, Y., Bockemühl, T., Büschges, A., and Scott, K. (2020). Two brain pathways initiate distinct forward walking programs in Drosophila. Neuron *108*, 469–485.e8. https://doi.org/10.1016/j.neuron.2020.07.032.
10. Akay, T., Tourtellotte, W.G., Arber, S., and Jessell, T.M. (2014). Degradation of mouse locomotor pattern in the absence of proprioceptive sensory feedback. Proc. Natl. Acad. Sci. USA *111*, 16877–16882. https://doi.org/10.1073/pnas.1419045111.
11. Mendes, C.S., Bartos, I., Akay, T., Márka, S., and Mann, R.S. (2013). Quantification of gait parameters in freely walking wild type and sensory deprived Drosophila melanogaster. eLife *2*, e00231. https://doi.org/10.7554/eLife.00231.
12. Smith, S.A., and Shepherd, D. (1996). Central afferent projections of proprioceptive sensory neurons in Drosophila revealed with the enhancer-trap technique. J. Comp. Neurol. *364*, 311–323. https://doi.org/10.1002/(SICI)1096-9861(19960108)364:2<311::AID-CNE9>3.0.CO;2-8.
13. Tuthill, J.C., and Wilson, R.I. (2016). Parallel transformation of tactile signals in central circuits of Drosophila. Cell *164*, 1046–1059. https://doi.org/10.1016/j.cell.2016.01.014.
14. Tsubouchi, A., Yano, T., Yokoyama, T.K., Murtin, C., Otsuna, H., and Ito, K. (2017). Topological and modality-specific representation of somatosensory information in the fly brain. Science *358*, 615–623. https://doi.org/10.1126/science.aan4428.
15. Li, J., Zhang, W., Guo, Z., Wu, S., Jan, L.Y., and Jan, Y.N. (2016). A defensive kicking behavior in response to mechanical stimuli mediated by Drosophila wing margin bristles. J. Neurosci. *36*, 11275–11282. https://doi.org/10.1523/JNEUROSCI.1416-16.2016.
16. Seeds, A.M., Ravbar, P., Chung, P., Hampel, S., Midgley, F.M., Jr., Mensh, B.D., and Simpson, J.H. (2014). A suppression hierarchy among

competing motor programs drives sequential grooming in Drosophila. eLife *3*, e02951. https://doi.org/10.7554/eLife.02951.

17. Vandervorst, P., and Ghysen, A. (1980). Genetic control of sensory connections in Drosophila. Nature *286*, 65–67. https://doi.org/10.1038/286065a0.
18. Siegler, M.V., and Burrows, M. (1986). Receptive fields of motor neurons underlying local tactile reflexes in the locust. J. Neurosci. *6*, 507–513. https://doi.org/10.1523/JNEUROSCI.06-02-00507.1986.
19. DeAngelis, B.D., Zavatone-Veth, J.A., Gonzalez-Suarez, A.D., and Clark, D.A. (2020). Spatiotemporally precise optogenetic activation of sensory neurons in freely walking Drosophila. eLife *9*, e54183. https://doi.org/10.7554/eLife.54183.
20. Murphey, R.K., Possidente, D., Pollack, G., and Merritt, D.J. (1989). Modality-specific axonal projections in the CNS of the flies Phormia and Drosophila. J. Comp. Neurol. *290*, 185–200. https://doi.org/10.1002/cne.902900203.
21. Burrows, M. (1996). The Neurobiology of an Insect Brain (Oxford University Press).
22. Nagayama, T., and Burrows, M. (1990). Input and output connections of an anteromedial group of spiking local interneurons in the metathoracic ganglion of the locust. J. Neurosci. *10*, 785–794. https://doi.org/10.1523/JNEUROSCI.10-03-00785.1990.
23. Akay, T., and Büschges, A. (2006). Load signals assist the generation of movement-dependent reflex reversal in the femur-tibia joint of stick insects. J. Neurophysiol. *96*, 3532–3537. https://doi.org/10.1152/jn.00625.2006.
24. Bässler, U., and Büschges, A. (1998). Pattern generation for stick insect walking movements–multisensory control of a locomotor program. Brain Res. Brain Res. Rev. *27*, 65–88. https://doi.org/10.1016/s0165-0173(98)00006-x.
25. Berkowitz, A., and Laurent, G. (1996). Central generation of grooming motor patterns and interlimb coordination in locusts. J. Neurosci. *16*, 8079–8091. https://doi.org/10.1523/JNEUROSCI.16-24-08079.1996.
26. Borgmann, A., Toth, T.I., Gruhn, M., Daun-Gruhn, S., and Büschges, A. (2011). Dominance of local sensory signals over inter-segmental effects in a motor system: experiments. Biol. Cybern. *105*, 399–411. https://doi.org/10.1007/s00422-012-0473-y.
27. Jenett, A., Rubin, G.M., Ngo, T.T.B., Shepherd, D., Murphy, C., Dionne, H., Pfeiffer, B.D., Cavallaro, A., Hall, D., Jeter, J., et al. (2012). A GAL4-driver line resource for Drosophila neurobiology. Cell Rep. *2*, 991–1001. https://doi.org/10.1016/j.celrep.2012.09.011.
28. Nottebohm, E., Usui, A., Therianos, S., Kimura, K., Dambly-Chaudière, C., and Ghysen, A. (1994). The gene poxn controls different steps of the formation of chemosensory organs in Drosophila. Neuron *12*, 25–34. https://doi.org/10.1016/0896-6273(94)90149-x.
29. Koh, T.W., He, Z., Gorur-Shandilya, S., Menuz, K., Larter, N.K., Stewart, S., and Carlson, J.R. (2014). The Drosophila IR20a clade of ionotropic receptors are candidate taste and pheromone receptors. Neuron *83*, 850–865. https://doi.org/10.1016/j.neuron.2014.07.012.
30. Court, R., Namiki, S., Armstrong, J.D., Börner, J., Card, G., Costa, M., Dickinson, M., Duch, C., Korff, W., Mann, R., et al. (2020). A systematic nomenclature for the Drosophila ventral nerve cord. Neuron *107*, 1071–1079.e2. https://doi.org/10.1016/j.neuron.2020.08.1005.
31. Kain, P., and Dahanukar, A. (2015). Secondary taste neurons that convey sweet taste and starvation in the Drosophila brain. Neuron *85*, 819–832. https://doi.org/10.1016/j.neuron.2015.01.005.
32. Gao, Q., Yuan, B., and Chess, A. (2000). Convergent projections of Drosophila olfactory neurons to specific glomeruli in the antennal lobe. Nat. Neurosci. *3*, 780–785. https://doi.org/10.1038/77680.
33. Kendroud, S., Bohra, A.A., Kuert, P.A., Nguyen, B., Guillermin, O., Sprecher, S.G., Reichert, H., VijayRaghavan, K., and Hartenstein, V. (2018). Structure and development of the subesophageal zone of the Drosophila brain. II. Sensory compartments. J. Comp. Neurol. *526*, 33–58. https://doi.org/10.1002/cne.24316.
34. Klapoetke, N.C., Murata, Y., Kim, S.S., Pulver, S.R., Birdsey-Benson, A., Cho, Y.K., Morimoto, T.K., Chuong, A.S., Carpenter, E.J., Tian, Z., et al. (2014). Independent optical excitation of distinct neural populations. Nat. Methods *11*, 338–346. https://doi.org/10.1038/nmeth.2836.
35. Eaton, R.C. (2013). Neural Mechanisms of Startle Behavior (Springer).
36. Hampel, S., McKellar, C.E., Simpson, J.H., and Seeds, A.M. (2017). Simultaneous activation of parallel sensory pathways promotes a grooming sequence in Drosophila. eLife *6*, e28804. https://doi.org/10.7554/eLife.28804.
37. Burrows, M. (1987). Parallel processing of proprioceptive signals by spiking local interneurons and motor neurons in the locust. J. Neurosci. *7*, 1064–1080. https://doi.org/10.1523/JNEUROSCI.07-04-01064.1987.
38. Kim, J., Chung, Y.D., Park, D.Y., Choi, S., Shin, D.W., Soh, H., Lee, H.W., Son, W., Yim, J., Park, C.S., et al. (2003). A TRPV family ion channel required for hearing in Drosophila. Nature *424*, 81–84. https://doi.org/10.1038/nature01733.
39. Ravbar, P., Zhang, N., and Simpson, J.H. (2021). Behavioral evidence for nested central pattern generator control of Drosophila grooming. eLife *10*, e71508. https://doi.org/10.7554/eLife.71508.
40. Israel, S., Rozenfeld, E., Weber, D., Huetteroth, W., and Parnas, M. (2022). Olfactory stimuli and moonwalker SEZ neurons can drive backward locomotion in Drosophila. Curr. Biol. *32*, 1131–1149.e7. https://doi.org/10.1016/j.cub.2022.01.035.
41. Mendes, C.S., Rajendren, S.V., Bartos, I., Márka, S., and Mann, R.S. (2014). Kinematic responses to changes in walking orientation and gravitational load in Drosophila melanogaster. PLoS One *9*, e109204. https://doi.org/10.1371/journal.pone.0109204.
42. Cabrita, A., Medeiros, A.M., Pereira, T., Rodrigues, A.S., Kranendonk, M., and Mendes, C.S. (2022). Motor dysfunction in Drosophila melanogaster as a biomarker for developmental neurotoxicity. iScience *25*, 104541. https://doi.org/10.1016/j.isci.2022.104541.
43. Strauss, R., and Heisenberg, M. (1990). Coordination of legs during straight walking and turning in Drosophila melanogaster. J. Comp. Physiol. A *167*, 403–412. https://doi.org/10.1007/BF00192575.
44. Wosnitza, A., Bockemühl, T., Dübbert, M., Scholz, H., and Büschges, A. (2013). Inter-leg coordination in the control of walking speed in Drosophila. J. Exp. Biol. *216*, 480–491. https://doi.org/10.1242/jeb.078139.
45. Gowda, S.B.M., Paranjpe, P.D., Reddy, O.V., Thiagarajan, D., Palliyil, S., Reichert, H., and VijayRaghavan, K. (2018). GABAergic inhibition of leg motoneurons is required for normal walking behavior in freely moving Drosophila. Proc. Natl. Acad. Sci. USA *115*, E2115–E2124. https://doi.org/10.1073/pnas.1713869115.
46. Szczecinski, N.S., Bockemühl, T., Chockley, A.S., and Büschges, A. (2018). Static stability predicts the continuum of interleg coordination patterns in Drosophila. J. Exp. Biol. *221*, jeb189142. https://doi.org/10.1242/jeb.189142.
47. Cruse, H., Kindermann, T., Schumm, M., Dean, J., and Schmitz, J. (1998). Walknet-a biologically inspired network to control six-legged walking. Neural Netw. *11*, 1435–1447. https://doi.org/10.1016/s0893-6080(98)00067-7.
48. Dürr, V., Schmitz, J., and Cruse, H. (2004). Behaviour-based modelling of hexapod locomotion: linking biology and technical application. Arthropod Struct. Dev. *33*, 237–250. https://doi.org/10.1016/j.asd.2004.05.004.
49. Cruse, H., and Bartling, C. (1995). Movement of joint angles in the legs of a walking insect, Carausius morosus. Journal of Insect Physiology *41*, 761–771. https://doi.org/10.1016/0022-1910(95)00032-P.
50. Barrios, N., Farias, M., and Moita, M.A. (2021). Threat induces cardiac and metabolic changes that negatively impact survival in flies. Curr. Biol. *31*, 5462–5472.e4. https://doi.org/10.1016/j.cub.2021.10.013.
51. Mathis, A., Mamidanna, P., Cury, K.M., Abe, T., Murthy, V.N., Mathis, M.W., and Bethge, M. (2018). DeepLabCut: markerless pose estimation of user-defined body parts with deep learning. Nat. Neurosci. *21*, 1281–1289. https://doi.org/10.1038/s41593-018-0209-y.

52. Venkatasubramanian, L., Guo, Z., Xu, S., Tan, L., Xiao, Q., Nagarkar-Jaiswal, S., and Mann, R.S. (2019). Stereotyped terminal axon branching of leg motor neurons mediated by IgSF proteins DIP-α and Dpr10. eLife *8*, e42692. https://doi.org/10.7554/eLife.42692.

53. Feng, K., Sen, R., Minegishi, R., Dübbert, M., Bockemühl, T., Büschges, A., and Dickson, B.J. (2020). Distributed control of motor circuits for backward walking in Drosophila. Nat. Commun. *11*, 6166. https://doi.org/10.1038/s41467-020-19936-x.

54. Büschges, A. (2005). Sensory control and organization of neural networks mediating coordination of multisegmental organs for locomotion. J. Neurophysiol. *93*, 1127–1135. https://doi.org/10.1152/jn.00615.2004.

55. Soler, C., Daczewska, M., Da Ponte, J.P., Dastugue, B., and Jagla, K. (2004). Coordinated development of muscles and tendons of the Drosophila leg. Development *131*, 6041–6051. https://doi.org/10.1242/dev.01527.

56. Heredia, F., Volonté, Y., Pereirinha, J., Fernandez-Acosta, M., Casimiro, A.P., Belém, C.G., Viegas, F., Tanaka, K., Menezes, J., Arana, M., et al. (2021). The steroid-hormone ecdysone coordinates parallel pupariation neuromotor and morphogenetic subprograms via epidermis-to-neuron Dilp8-Lgr3 signal induction. Nat. Commun. *12*, 3328. https://doi.org/10.1038/s41467-021-23218-5.

57. Ramdya, P., Lichocki, P., Cruchet, S., Frisch, L., Tse, W., Floreano, D., and Benton, R. (2015). Mechanosensory interactions drive collective behaviour in Drosophila. Nature *519*, 233–236. https://doi.org/10.1038/nature14024.

58. Kim, S.E., Coste, B., Chadha, A., Cook, B., and Patapoutian, A. (2012). The role of Drosophila Piezo in mechanical nociception. Nature *483*, 209–212. https://doi.org/10.1038/nature10801.

59. He, J., Li, B., Han, S., Zhang, Y., Liu, K., Yi, S., Liu, Y., and Xiu, M. (2022). Drosophila as a model to study the mechanism of nociception. Front. Physiol. *13*, 854124. https://doi.org/10.3389/fphys.2022.854124.

60. Hampel, S., Franconville, R., Simpson, J.H., and Seeds, A.M. (2015). A neural command circuit for grooming movement control. eLife *4*, e08758. https://doi.org/10.7554/eLife.08758.

61. Jordan, K.W., Morgan, T.J., and Mackay, T.F.C. (2006). Quantitative trait loci for locomotor behavior in Drosophila melanogaster. Genetics *174*, 271–284. https://doi.org/10.1534/genetics.106.058099.

62. Yamamoto, A., Zwarts, L., Callaerts, P., Norga, K., Mackay, T.F.C., and Anholt, R.R.H. (2008). Neurogenetic networks for startle-induced locomotion in Drosophila melanogaster. Proc. Natl. Acad. Sci. USA *105*, 12393–12398. https://doi.org/10.1073/pnas.0804889105.

63. Norga, K.K., Gurganus, M.C., Dilda, C.L., Yamamoto, A., Lyman, R.F., Patel, P.H., Rubin, G.M., Hoskins, R.A., Mackay, T.F., and Bellen, H.J. (2003). Quantitative analysis of bristle number in Drosophila mutants identifies genes involved in neural development. Curr. Biol. *13*, 1388–1396. https://doi.org/10.1016/s0960-9822(03)00546-3.

64. Card, G., and Dickinson, M. (2008). Performance trade-offs in the flight initiation of Drosophila. J. Exp. Biol. *211*, 341–353. https://doi.org/10.1242/jeb.012682.

65. von Reyn, C.R., Breads, P., Peek, M.Y., Zheng, G.Z., Williamson, W.R., Yee, A.L., Leonardo, A., and Card, G.M. (2014). A spike-timing mechanism for action selection. Nat. Neurosci. *17*, 962–970. https://doi.org/10.1038/nn.3741.

66. Troconis, E.L., Ordoobadi, A.J., Sommers, T.F., Aziz-Bose, R., Carter, A.R., and Trapani, J.G. (2017). Intensity-dependent timing and precision of startle response latency in larval zebrafish. J. Physiol. *595*, 265–282. https://doi.org/10.1113/JP272466.

67. Card, G., and Dickinson, M.H. (2008). Visually mediated motor planning in the escape response of Drosophila. Curr. Biol. *18*, 1300–1307. https://doi.org/10.1016/j.cub.2008.07.094.

68. Browne, L.E., Latremoliere, A., Lehnert, B.P., Grantham, A., Ward, C., Alexandre, C., Costigan, M., Michoud, F., Roberson, D.P., Ginty, D.D., and Woolf, C.J. (2017). Time-resolved fast mammalian behavior reveals the complexity of protective pain responses. Cell Rep. *20*, 89–98. https://doi.org/10.1016/j.celrep.2017.06.024.

69. Clarke, R.W., and Harris, J. (2004). The organization of motor responses to noxious stimuli. Brain Res. Brain Res. Rev. *46*, 163–172. https://doi.org/10.1016/j.brainresrev.2004.07.005.

70. Sen, R., Wu, M., Branson, K., Robie, A., Rubin, G.M., and Dickson, B.J. (2017). Moonwalker descending neurons mediate visually evoked retreat in Drosophila. Curr. Biol. *27*, 766–771. https://doi.org/10.1016/j.cub.2017.02.008.

71. Akay, T., Ludwar, B.Ch., Göritz, M.L., Schmitz, J., and Büschges, A. (2007). Segment specificity of load signal processing depends on walking direction in the stick insect leg muscle control system. J. Neurosci. *27*, 3285–3294. https://doi.org/10.1523/JNEUROSCI.5202-06.2007.

72. Bässler, U. (2012). Neural Basis of Elementary Behavior in Stick Insects*10* (Springer Science & Business Media).

73. Tóth, T.I., Knops, S., and Daun-Gruhn, S. (2012). A neuromechanical model explaining forward and backward stepping in the stick insect. J. Neurophysiol. *107*, 3267–3280. https://doi.org/10.1152/jn.01124.2011.

74. Pearson, K.G. (1972). Central programming and reflex control of walking in the cockroach. J. Exp. Biol. *56*, 173–193. https://doi.org/10.1242/jeb.56.1.173.

75. Ryckebusch, S., and Laurent, G. (1993). Rhythmic patterns evoked in locust leg motor neurons by the muscarinic agonist pilocarpine. J. Neurophysiol. *69*, 1583–1595. https://doi.org/10.1152/jn.1993.69.5.1583.

76. Büschges, A. (1995). Role of local nonspiking interneurons in the generation of rhythmic motor activity in the stick insect. J. Neurobiol. *27*, 488–512. https://doi.org/10.1002/neu.480270405.

77. Yellman, C., Tao, H., He, B., and Hirsh, J. (1997). Conserved and sexually dimorphic behavioral responses to biogenic amines in decapitated Drosophila. Proc. Natl. Acad. Sci. USA *94*, 4131–4136. https://doi.org/10.1073/pnas.94.8.4131.

78. Chrachri, A., and Clarac, F. (1987). Induction of rhythmic activity in motoneurons of crayfish thoracic ganglia by cholinergic agonists. Neurosci. Lett. *77*, 49–54. https://doi.org/10.1016/0304-3940(87)90605-7.

79. Johnston, R.M., and Levine, R.B. (2002). Thoracic leg motoneurons in the isolated CNS of adult Manduca produce patterned activity in response to pilocarpine, which is distinct from that produced in larvae. Invert. Neurosci. *4*, 175–192. https://doi.org/10.1007/s10158-002-0019-4.

80. Pearson, K.G., and Fourtner, C.R. (1975). Nonspiking interneurons in walking system of the cockroach. J. Neurophysiol. *38*, 33–52. https://doi.org/10.1152/jn.1975.38.1.33.

81. Weiland, G., Bässler, U., and Brunner, M. (1986). A biological feedback control system with electronic input: the artificially closed femur-tibia control system of stick insects. J. Exp. Biol. *120*, 369–385. https://doi.org/10.1242/jeb.120.1.369.

82. Bässler, U. (1983). Neural Basis of Elementary Behavior in Stick Insects (Springer-Verlag).

83. Bässler, U., and Nothof, U. (1994). Gain control in a proprioceptive feedback loop as a prerequisite for working close to instability. J. Comp. Physiol. A *175*, 23–33.

84. Ji, H., Fouad, A.D., Teng, S., Liu, A., Alvarez-Illera, P., Yao, B., Li, Z., and Fang-Yen, C. (2021). Phase response analyses support a relaxation oscillator model of locomotor rhythm generation in Caenorhabditis elegans. eLife *10*, e69905. https://doi.org/10.7554/eLife.69905.

85. Phelps, J.S., Hildebrand, D.G.C., Graham, B.J., Kuan, A.T., Thomas, L.A., Nguyen, T.M., Buhmann, J., Azevedo, A.W., Sustar, A., Agrawal, S., et al. (2021). Reconstruction of motor control circuits in adult Drosophila using automated transmission electron microscopy. Cell *184*, 759–774.e8. https://doi.org/10.1016/j.cell.2020.12.013.

86. Strausfeld, N.J., Bassemir, U., Singh, R.N., and Bacon, J.P. (1984). Organizational principles of outputs from dipteran brains. J. Insect Physiol. *30*, 73–93. https://doi.org/10.1016/0022-1910(84)90109-4.

87. Bidaye, S.S., Machacek, C., Wu, Y., and Dickson, B.J. (2014). Neuronal control of Drosophila walking direction. Science *344*, 97–101. https://doi.org/10.1126/science.1249964.

88. Namiki, S., Dickinson, M.H., Wong, A.M., Korff, W., and Card, G.M. (2018). The functional organization of descending sensory-motor pathways in Drosophila. eLife *7*, e34272. https://doi.org/10.7554/eLife.34272.

89. Juvin, L., Le Gal, J.-P., Simmers, J., and Morin, D. (2012). Cervicolumbar coordination in mammalian quadrupedal locomotion: role of spinal thoracic circuitry and limb sensory inputs. J. Neurosci. *32*, 953–965. https://doi.org/10.1523/JNEUROSCI.4640-11.2012.

90. Mantziaris, C., Bockemühl, T., Holmes, P., Borgmann, A., Daun, S., and Büschges, A. (2017). Intra-and intersegmental influences among central pattern generating networks in the walking system of the stick insect. J. Neurophysiol. *118*, 2296–2310. https://doi.org/10.1152/jn.00321.2017.

91. Wu, M., Nern, A., Williamson, W.R., Morimoto, M.M., Reiser, M.B., Card, G.M., and Rubin, G.M. (2016). Visual projection neurons in the Drosophila lobula link feature detection to distinct behavioral programs. eLife *5*, e21022. https://doi.org/10.7554/eLife.21022.

92. Schindelin, J., Arganda-Carreras, I., Frise, E., Kaynig, V., Longair, M., Pietzsch, T., Preibisch, S., Rueden, C., Saalfeld, S., Schmid, B., et al. (2012). Fiji: an open-source platform for biological-image analysis. Nat. Methods *9*, 676–682. https://doi.org/10.1038/nmeth.2019.

93. zur Lage, P.I., Powell, L.M., Prentice, D.R.A., McLaughlin, P., and Jarman, A.P. (2004). EGF receptor signaling triggers recruitment of Drosophila sense organ precursors by stimulating proneural gene autoregulation. Dev. Cell *7*, 687–696. https://doi.org/10.1016/j.devcel.2004.09.015.

94. Zecca, M., and Struhl, G. (2007). Control of Drosophila wing growth by the vestigial quadrant enhancer. Development *134*, 3011–3020. https://doi.org/10.1242/dev.006445.

95. Lopes, G., Bonacchi, N., Frazão, J., Neto, J.P., Atallah, B.V., Soares, S., Moreira, L., Matias, S., Itskov, P.M., Correia, P.A., et al. (2015). Bonsai: an event-based framework for processing and controlling data streams. Front. Neuroinform. *9*, 7. https://doi.org/10.3389/fninf.2015.00007.

96. Sink, H., and Hartenstein, V. (2006). The muscle pattern of Drosophila. In Muscle Development in Drosophila (Springer), pp. 8–27.

Please cite this article in press as: Medeiros et al., Mechanosensory bristles mediate avoidance behavior by triggering sustained local motor activity in *Drosophila melanogaster*, Current Biology (2024), https://doi.org/10.1016/j.cub.2024.05.021

STAR★METHODS

KEY RESOURCES TABLE

REAGENT or RESOURCE	SOURCE	IDENTIFIER
Antibodies		
Mouse anti-nc82	DSHB	RRID: AB_2314866
Donkey Anti-mouse Alexa 647	Jackson ImmunoResearch	RRID: AB_2340862
Chemicals, peptides, and recombinant proteins		
All-trans-Retinal	Sigma-Aldrich	MFCD00001550
Deposited data		
Tracked and processed behavioral data	This paper	https://doi.org/10.5281/zenodo.10798135
Experimental models: Organisms/strains		
R65D12-GAL4(attP2)	BDSC	RRID: BDSC_49611
R77E09-GAL4(attP2)	BDSC	RRID: BDSC_39970
R85A07-GAL4(attP2)	BDSC	RRID: BDSC_40413
R45D07-GAL4(attP2)	BDSC	RRID: BDSC_49562
R54A11-GAL4(attP2)	BDSC	RRID: BDSC_49588
R39A11-GAL4(attP2)	BDSC	RRID: BDSC_50034
R64D07-GAL4(attP2)	BDSC	RRID: BDSC_39304
R50A05-GAL4(attP2)	BDSC	RRID: BDSC_38721
R22E04-GAL4(attP2)	BDSC	RRID: BDSC_49873
R79E02-GAL4(attP2)	BDSC	RRID: BDSC_48623
pBDP-GAL4UW(w[1118]; P{GAL4.1Uw}attp2) (empty-GAL4).	BDSC	RRID: BDSC_68384
Piezo-GAL4	BDSC	RRID: BDSC_58771
Ato1.9-flp	This paper	N/A
Vg^{BE} -flp	This paper	N/A
dac^{RE}-flp	Mendes et al.[11]	N/A
UAS-FRT-stop-FRT- CsChrimson-mVenus	Gift from Gerry Rubin. Wu et al.[91]	N/A
lexO-GCaMP6f/;mhc-lexA:LHV2, lexO-Cherry/SM6^Tm6b	Heredia et al.[56]	N/A
ey-flp	BDSC	RRID: BDSC_5576
13xLexAop2-GCaMP6f (attp5)	BDSC	RRID: BDSC_44277
dac^{RE}-flp;UAS-FRT-stop-FRT-CsChrimson-mVenus (VK5), R65D12-GAL4 (attP2)	This paper	N/A
W[1118];;UAS(FRT.stop)mCD8-GFP, UAS(FRT.stop)mCD8-GFP	BDSC	RRID: BDSC_30032
W[1118];UAS(FRT.stop)mCD8-GFP/CyO	BDSC	RRID: BDSC_30125
Software and algorithms		
FlyWalker	Mendes et al.[11]	https://doi.org/10.7554/eLife.00231
Fiji	Schindelin et al.[92]	https://fiji.sc
MATLAB 2020	Mathworks	https://www.mathworks.com/products/matlab.html
Imaris 9.5	Oxford instruments	https://imaris.oxinst.com/
RStudio 1.1.442	RStudio	https://www.rstudio.com
GraphPad Prism v6	GraphPad	https://www.graphpad.com/scientificsoftware/prism
Python 3.6.4 Anaconda	Anaconda	https://www.anaconda.com/distribution/
Data processing - Residuals Analysis	Cabrita et al.[42]	https://github.com/NeurogeneLocomotion/Data-Processing—Residuals-Analysis.git

(*Continued on next page*)

Please cite this article in press as: Medeiros et al., Mechanosensory bristles mediate avoidance behavior by triggering sustained local motor activity in *Drosophila melanogaster*, Current Biology (2024), https://doi.org/10.1016/j.cub.2024.05.021

Continued

REAGENT or RESOURCE	SOURCE	IDENTIFIER
Data Visualization - Outlier removal and Heatmap	Cabrita et al.[42]	https://github.com/NeurogeneLocomotion/Data-Visualization–Outlier-removal-and-Heatmap.git
Data visualization - Principal Component Analysis	Cabrita et al.[42]	https://github.com/NeurogeneLocomotion/Principal-Component-Analysis.git
Data visualization - Speed and Cumulative Distances	This paper	https://github.com/NeurogeneLocomotion/Flytrack_Trajectories_Speed_CumulativeDistance
Data visualization – Leg Trajectory analysis of fly on the ball	This paper	https://github.com/NeurogeneLocomotion/Leg-Trajectory-Analysis
Data visualization - Muscle activity analysis Fluorescence plots	This paper	https://github.com/NeurogeneLocomotion/Muscle-activity-analysis_Fluorescence-Plots
Data visualization - FlyTrack Raster plots	This paper	https://github.com/NeurogeneLocomotion/Flytrack_RasterPlots
Data Analysis - Stance phase Leg retraction	This paper	https://github.com/NeurogeneLocomotion/Analysis-of-Stance-Phase-Leg-retraction
Data Analysis – Laser Wall avoidance analysis	This paper	https://github.com/NeurogeneLocomotion/Laser-wall-analysis
Data Analysis – Individual laser interaction behavior	This paper	https://github.com/NeurogeneLocomotion/Ind_laser_interaction_behavior

RESOURCE AVAILABILITY

Lead contact

Further information and requests for resources and reagents should be directed to and will be fulfilled by the lead contact, César S. Mendes (cesar.mendes@nms.unl.pt).

Materials availability

Fly lines generated in this study are available upon request from the lead contact.

Data and code availability

- All data reported in this paper have been deposited at Zenodo and is publicly available as of the date of publication.
- All original code has been deposited at Github and is publicly available as of the date of publication. Links are listed in the key resources table.
- Any additional information required to reanalyze the data reported in this paper is available from the lead contact upon request.

EXPERIMENTAL MODEL AND SUBJECT DETAILS

Fly stocks

Flies were housed in a 25°C incubator with 50-70% humidity. The GAL4 lines from the Janelia Flylight Collection were: R65D12-GAL4(attP2), R77E09-GAL4(attP2), R85A07-GAL4(attP2), R45D07-GAL4(attP2), R54A11-GAL4(attP2), R39A11-GAL4(attP2) and R64D07-GAL4(attP2), R50A05-GAL4(attP2), R22E04-GAL4(attP2), R79E02-GAL4(attP2) and pBDP-GAL4UW (w[1118];P{GAL4.1Uw}attp2) (empty-GAL4). Piezo-GAL4 line was obtained from Bloomington (BL58771). Ato1.9-flp and Vg^{BE} -flp were generated by TOPO cloning into an entry clone the 1.9kb enhancer fragment from the regulatory region of atonal[93] and the boundary enhancer of vestigial (Vg^{BE})[94] (a gift from Mirian Zecca), respectively. Both entry clones were subjected to a Gateway reaction into a flp destination plasmid. Transgenic lines were generated by standard procedures in a *yw* background. The dac^{RE}-flp was used in previously.[11] UAS-FRT-stop-FRT- CsChrimson-mVenus was a gift from Gerry Rubin.[91] UAS-FRT-stop-FRT-GFP, Lexop-GCaMP6f and ey-flp lines were obtained from the Bloomington Stock Center. For the calcium imaging in leg muscles we used lexO-GCamp6f;mhc-lexA:LHV2,lexO-Cherry/SM6^Tm6b[56] and the recombinant line dac^{RE}-flp;UAS-FRT-stop-FRT-CsChrimson-mVenus (VK5), R65D12-GAL4 (attP2). All flies used in this study were non-virgin females between 1 and 7 days post-eclosion. Prior to experimentation, all flies were manipulated under cold anesthesia and allowed to recover for at least 24 hours.

Please cite this article in press as: Medeiros et al., Mechanosensory bristles mediate avoidance behavior by triggering sustained local motor activity in *Drosophila melanogaster*, Current Biology (2024), https://doi.org/10.1016/j.cub.2024.05.021

METHOD DETAILS

Behavior setup and optogenetic activation of mechanosensory structures

The open-field behavior arena for optogenetic stimulation was custom-built from a 3 mm opaque white and black acrylic sheet using a laser cutter. The circular arena comprised a diameter of 54 mm and was surrounded by evenly distributed six deep 655 nm red LEDs (LUXEON Rebel LEDs), providing a stimulation power of 0.016 mW/mm2 (Figure 1C). The edge of the arena was surrounded by water to prevent flies accessing the walls. The top of the arena (transparent acrylic) was covered with Sigmacote (Sigma-Aldrich). A white LED array was placed under the arena to serve as backlight. Flies were imaged from above using a camera (Flea3-USB3, Point Grey, Teledyne FLIR LLC) equipped with a 12 mm Computar (Commack, NY) lens covered with a 600nm, OD 4.0 Shortpass Filter (Edmund optics, Barrington, NJ) to block optogenetic stimulation light.

For the experiments in Figure 1, we used 1-7 day old females, comprising 20 control flies (empty-GAL4), and 20 flies expressing CsChrimson in leg mechanosensory bristles. Flies were bred and kept in food infused with all trans-Retinal (Final Concentration 0.4 mM; R2500, Sigma-Aldrich). Single flies were aspirated into the chamber. We waited for a spontaneous pause in behavior (no walking or grooming) and manually delivered a single pulse stimulation of 100ms. Imaging continued for at least 20 seconds after stimulation. For decapitated fly experiments, flies were anesthetized on a cold plate and their head was cut off. After surgery, flies were kept in an empty vial for 1-5 minutes prior to testing.

For the experiments in Figure 6, we used a rectangular 3D-printed custom arena crossed in the middle by a red laser line (650 nm, 5mW). Flies were placed in one side of the arena (side A) and allowed to move freely. Each trial lasted 3 minutes.

In the experiments in Figures 7A and 7B, where we activated the back and front legs of headless and head-intact flies, we used the same arena, but this time we waited until flies were immobile and moved the laser line until it touched the back or front of the fly.

Video acquisition and Tracking

The video image was acquired at 30 Hz (1200 x 1210) using Fly capture software. Image segmentation was performed by custom software in python using OpenCV. Two main features were extracted from the videos: fly position (X and Y coordinates) and pixel change around the fly. Positions were calculated from the centroid of an ellipse fitted to the fly by background subtraction. The pixel change was quantified by calculating the number of active pixels in a 100x100 pixel region surrounding the centroid. A pixel was considered to be active if it recorded a change higher than 10 intensity levels. The fly distance and speed were calculated for each frame using fly position x and y coordinates.

For the analysis of the interaction of the flies with the laser in Figure 6, tracking was performed using FlyTracker (Caltech), which extracts the body centroid, axis and orientation.

Behavioral classifiers

We used velocity and pixel change features to automatically classify behavioral states. We classified fly behavior into four categories: Walking, Grooming, Stopping and Leg Movement. A fly is considered to be walking if its average speed is higher than 1.9mm/s. Grooming is detected when the velocity of the fly is lower than 1.9mm/s and average pixel change of a section of 8 frames is above 180 pixel/s. We classified as leg displacement the movement in which velocity is lower than 1.9mm/s and average pixel change of a section of 8 frames is between 30 and 180 pixel/s. Finally, a fly is considered to be immobile when velocity is lower than 1.9 and pixel change is lower than 30 pixel/s. Thresholds were determined and confirmed by manual annotations of fly behavior (% of efficacy). Later, walking behavior was either classified into coordinated or uncoordinated walking by visual inspection (Figures 2 and S2).

For the analysis of individual laser interactions, we selected moments where the fly was in contact with the laser. We considered the fly touched the laser when in less than 2mm proximity with the area of highest laser intensity. This extra threshold was set to account for the fact that we are tracking the centroid of the body, but flies can sense the laser beam with their legs. To classify different behaviors, we used spatial and temporal thresholds; we considered the flies '*move away*' from the laser if they left the peri-laser zone (3mm above or below the area of high laser intensity) in less than 1 second; stayed in '*Peri-laser zone*' if they do not leave the area surrounding the laser; stayed in '*Laser* zone' if they were inside the high intensity laser are after one second; and '*Cross*' if they crossed to the other side of the laser. To compute the angles of the fly after laser interactions we used FlyTracker data, which provides the orientation of the flies in radians (where 0 represents a parallel position relative to the laser, with flies oriented to the right). After converting radians to degrees, we adjusted all entry angles to fall between 0 and 90° in relation to the laser. Additionally, we adjusted the quadrant of the exit angles depending on the transformation of the entry angle. If an entry angle underwent a transformation, we swapped the quadrant of the corresponding exit angle. Angular speed was determined by calculating the average angle variation over 5 frames following laser interaction. Finally, velocity was calculated considering the orientation of the fly, if the fly moved backwards the speed was recorded as negative.

fTIR imaging and FlyWalker software

For the analysis of walking behavior upon stimulation of sensory structures, a new arena comprising 12 LEDs (Deep red 655nm, Luxeon Rebel LED) was incorporated in the previously described fTIR setup,[11] rendering a stimulation power of 0.014 mW/mm^2. Flies were placed in the FlyWalker arena and a 100ms pulse of red light was given. Each fly only received one pulse. In experiments involving headless flies, their heads were reattached to the thorax using UV-curable glue (Loctite 3104, Henkel Adhesives) to facilitate accurate body tracking and preserve the fly's body weight and center of mass (COM).[46] The walking kinematics of flies after

Please cite this article in press as: Medeiros et al., Mechanosensory bristles mediate avoidance behavior by triggering sustained local motor activity in *Drosophila melanogaster*, Current Biology (2024), https://doi.org/10.1016/j.cub.2024.05.021

stimulation were quantified using FlyWalker software package. We identified stance and stance-like phases by detecting an fTIR signal, indicating an interaction between the fly leg and the glass substrate, and swing phase as the absence of this signal.[11] Two additional parameters called *Non-compliant Index* and *Stance Phase Leg Retraction* were added to the previously published kinematics parameters. *Non-compliant Index* is defined as the fraction of frames in a video in which the fly displays non-compliant leg combinations. Non-canonical stance combinations correspond to patterns that do not fit either of the idealized tripod, tetrapod and wave gaits.[11,41]

The *Stance Phase Leg Retraction* measures the direction of the leg movement in relation to the body. It is calculated by finding the difference between y coordinates of AEP (Anterior extreme position) to the y coordinates of PEP (Posterior extreme position) for each step. The values were normalized to the body length (*b.u.*). When the *Stance Phase Leg Retraction* value is positive, it indicates that the leg moved from an anterior to posterior movement in relation to the body during the stance phase. This forward-to-backward movement denotes a retraction of the leg. Negative values indicate leg posterior to anterior movement during the stance phase.

For experiments in Figures 7C–7E), we built a transparent plastic cover that encouraged the flies to walk on the FlyWalker glass. We waited for a spontaneous pause and stimulated either the back or the front part of the fly with the red laser line (650 nm, 5mW).

Tethered fly imaging

For imaging of leg angles in Figures 5A–5E, 7F, and 7G), we used 3-7 days-old females expressing CsChrimson in mechanosensory bristles, as above. Adult flies were kept in food infused with all trans-Retinal since the day of eclosion (Final Concentration 0.4 mM, R2500, Sigma-Aldrich). Flies were anaesthetized on ice, and either decapitated with scissors (Fine Scientific Tools) or left with head-intact. They were positioned on a cold plate with the thorax upwards and a wire was glued to the thorax with UV curable glue (Norland Optical Adhesives #81). Flies were fixed in the tethered set-up using the wire above a porexpam ball (4.5 mm diameter, painted with black paint (Posca Uni)), held in a custom-made 3D printed holder. Flies could freely pick up and walk on the ball, and if dropped, could regain it again. Animals were illuminated with an InfraRed LED (Thorlabs) and imaged with a PointGrey Camera (Flea3) with a Computar Macro-zoom lens and a long-pass filter, at a frame rate of 120 fps. Video capture was controlled using a custom-built Bonsai workflow.[95]

Each fly was allowed to recover for 5 minutes on the setup before the beginning of the experiment. For stimulation in Figures 5A–5E), we waited for a spontaneous pause in behavior and delivered a 100ms light stimulus via a single deep red LED (627nm), positioned 3 cm away from the fly, controlled using Bonsai.[95] Light power at the fly was 13.8 nm/cm^2, calibrated to produce a motor response in CsChrimson flies whilst not affecting flies in food lacking all trans-Retinal (data not shown).

Walking bouts were extracted from head-intact non-stimulated flies (either before stimulation or in sessions where no stimulation was delivered), and were manually classified as satisfying straight walking with at least 6 step cycles. In total, 8 walking bouts were used from three flies. In the head-intact and headless stimulation conditions for the '*early response*' and '*late response*' timepoint, we visually inspected videos and excluded timepoints where the flies were either still or performing grooming, as being non-informative for our question of limb coordination while walking. Total N was 11 (head-intact *early response*), 6 (head-intact *late response*) and 7 (decapitated *early response*).

For tethered experiments in Figures 7F and 7G, we used the same red laser line as described in the freely moving set-ups (650nm). We positioned the laser laterally to the fly, to illuminate either only the front or back legs. We waited for moments of immobility in decapitated flies and delivered a long laser pulse (1.5-2s).

All videos were analyzed using DeepLabCut.[51] 18 points were tracked in total; 3 body points (head, thorax and tail) and 5 points per leg (Body-Coxa; Coxa-Femur; Femur-Tibia; Tibia-Tarsus; and Tarsus-end). Here we considered the fusion between the trochanter and femur.[96] In Figure 5, we considered angles only from the T1 leg, since this leg is predominantly at a perpendicular angle to the imaging path and thus the angles could be accurately calculated in a 2D video; while for Figure 7G we did T3 tracking. Limb angles for tracked legs were calculated using Python.

For Figure 7F, effective body displacement was calculated using absolute horizontal ball displacement over the stimulation period, with a custom-written Bonsai software, and normalized the displacement to average fly body length.

Leg and VNC dissection and Mounting

To observe the morphology of leg sensory neurons, legs were dissected from the body in PBS. The legs were then fixed in PFA 4% overnight at 4°C. After fixation legs were washed 3x in 0.3% Triton-X in PBS for 20 minutes at room temperature and mounted in 70% glycerol. Brains and VNCs were fixed in PFA 4% for 20 minutes and dissected in PBS. Tissues were labeled with a primary antibody raised against brp (mouse nc82, 1:10; DSHB) followed by a secondary anti-mouse 647 (1:500; Jackson ImmunoResearch). Tissues were mounted in in 70% glycerol and scanned in a confocal microscope Zeiss (Oberkochen, Germany) LSM710 confocal microscope with a 40× objective.

In vivo calcium imaging during leg stimulation

Flies containing the following genotype: lexO-GCamp6f;mhc-lexA:LHV2,lexO-Cherry and dac^{RE}-flp;UAS-FRT-stop-FRT-CsChrimson-mVenus (VK5), R65D12-GAL4 (attP2) were anesthetized with ice for 3-5 min. Three ipsilateral legs were glued to a glass slide with UV-Curable glue. The body of the fly was immobilized using beeswax. GCaMP imaging was performed at 25°C on a Nikon/Andor Revolution XD spinning-disk confocal microscope with an EMCCD camera (iXon 897) using iQ 3.5 software and using a

20× CFI Super Fluor 20X 0.75 NA dry objective. Images were taken at the scan speed of 100ms per frame. A set of six deep red LEDs was paced around the fly to provide the 100ms red light pulse.

QUANTIFICATION AND STATISTICAL ANALYSIS

We extracted motor parameters using FlyWalker Software. Since many of the measured gait parameters vary with speed, we analyzed the data for these parameters by determining the best-fit regression model of each individual parameter with speed for the control experiment and then determining the residual values for each experimental group in relation to this regression model. Data was then expressed as the difference to the residual normalized line. Normalized data was previously tested for normality and homoscedasticity with Shapiro-Wilk and Levene tests. Statistical differences between experimental groups were determined using Kruskal-Wallis analysis of variance followed by Dunn's *post hoc* test (for non-normal distributions) or one-way-Anova followed by Tukey's *post hoc* test (for normal distributions). Data analysis was performed using custom Python scripts. Boxplots represent the median as the middle line, with the lower and upper edges of the boxes representing the 25% and 75% quartiles, respectively. Whiskers represent the range of the full data set, excluding outliers. Outliers are defined as any value that is 1.5 times the interquartile range below or above the 25% and 75% quartiles, respectively. For the boxplots in Figures 3 and 4 we used raw data not normalized to the control since Non-compliant index and Stance straightness parameters do not show a correlation with velocity (data not shown).

To have a more succinct representation of the data, we used Principal Component Analysis (PCA), an unsupervised dimensionality reduction method. PCA finds a linear projection of the data from a high-dimensional space onto a lower-dimensional subspace, while maximizing variance of the projected data, and thus retains meaningful information, resulting in a description of the data as a function of a smaller set of uncorrelated variables (or principal components). Data were first pre-processed by centering and scaling, after which the PCA algorithm computed the covariance matrix in order to determine the correlation between variables and calculated the eigenvectors and eigenvalues of the covariance matrix in order to identify the principal components. We chose the first three principal components to visualize the data. The first two components were chosen to generate a two-dimensional plot. Each dot in the plots corresponds to a video, representing these new abstract variables. Color-coded dots were used to distinguish specific groups. As such, clusters of dots reflect similar walking patterns, shared by the corresponding flies.[42]

In order to generate a GCaMP fluorescence line profile over time, we used Fiji software. To delineate the ROI Area of the depressor and levator muscle, we used the threshold tool and measured the mean fluorescence value for each frame using ROI Manager, a multimeasure tool. Fluorescence values for each muscle were normalized by subtracting the minimum value of each video and dividing by the maximum value, giving contraction values between 0 and 100%. Muscle contraction peaks were detected with a peak finding algorithm in Python. Peak width was calculated by subtracting fluorescence 20 percentage points from each peak value, and measuring the width of the signal that exceeded this value around each peak (Figure S5C).